การจำลองโครงสร้างอัลลอยโมลิบดินัมไดซัลไฟด์โดยใช้วิธีโครงสร้างเสมือนสุ่มแบบพิเศษ

นายวิรุฬติ พึ่งตระกูล

วิทยานิพนธ์นี้เป็นส่วนหนึ่งของการศึกษาตามหลักสูตรปริญญาวิทยาศาสตรมหาบัณฑิต
สาขาวิชาฟิสิกส์ ภาควิชาฟิสิกส์
คณะวิทยาศาสตร์ จุฬาลงกรณ์มหาวิทยาลัย
ปีการศึกษา 2559

MODEL OF MOLYBDENUM TUNGSTEN DISULFIDE ALLOY STRUCTURE USING SPECIAL QUASIRANDOM STRUCTURE METHOD

Mr. Wirunti Pungtrakoon

A Thesis Submitted in Partial Fulfillment of the Requirements
for the Degree of Master of Science Program in Physics
Department of Physics
Faculty of Science
Chulalongkorn University
Academic Year 2016

Thesis Title	MODEL OF MOLYBDENUM TUNGSTEN DISULFIDE ALLOY STRUCTURE USING SPECIAL QUASIRANDOM STRUCTURE METHOD
By	Mr. Wirunti Pungtrakoon
Field of Study	Physics
Thesis Advisor	Assistant Professor Thiti Bovornratanaraks
Thesis Co-Advisor	Associate Professor Udomsilp Pinsook

Accepted by the Faculty of Science, Chulalongkorn University in Partial Fulfillment of the Requirements for the Master's Degree

.....Dean of the Faculty of Science

(No data found)

THESIS COMMITTEE

.....Chairman

(Assistant Professor Rattachat Mongkolnavin)

.....Thesis Advisor

(Assistant Professor Thiti Bovornratanaraks)

.....Thesis Co-Advisor

(Associate Professor Udomsilp Pinsook)

.....Examiner

(Rangsima Chanphana)

.....External Examiner

(Sornthep Vannarat)

วิรุฬติ พึ่งตระกูล : การจำลองโครงสร้างอัลลอยโมลิบดินัมไดซัลไฟด์โดยใช้วิธีโครงสร้างเสมือนสุ่มแบบพิเศษ (MODEL OF MOLYBDENUM TUNGSTEN DISULFIDE ALLOY STRUCTURE USING SPECIAL QUASIRANDOM STRUCTURE METHOD) อ.ที่ปรึกษาวิทยานิพนธ์หลัก: ผศ. ดร.ธิติ บวรรัตนารักษ์, อ.ที่ปรึกษาวิทยานิพนธ์ร่วม: รศ. ดร.อุดม ศิลป์ ปิ่นสุข, 59 หน้า.

สารประกอบอัลลอยแบบแทนที่คือโครงสร้างผลึกที่มีความผิดปกติจากการแทนที่ด้วยธาตุโลหะอื่นบนสารประกอบ การศึกษาเบื้องต้นของโครงสร้างอัลลอยจำเป็นต้องใช้โครงสร้างที่มีขนาดใหญ่เพื่อให้มีลักษณะการกระจายตัวแบบสุ่มในโครงสร้างนั้นๆ โครงสร้างอัลลอย $A_{1-x}B_x$ ที่นำมาใช้ในการคำนวณคุณสมบัติต่างๆ ถูกสร้างขึ้นจากการสุ่มตำแหน่งของอะตอม A และ B ในโครงสร้างช่วงคาบขนาดใหญ่ อย่างไรก็ตามผลการจำลองด้วยวิธีดังกล่าวนี้มีข้อเสียมากมาย จึงมีแนวทางการออกแบบจำลองโครงสร้างผลึกที่ดีกว่าเรียกว่า โครงสร้างเสมือนสุ่มแบบพิเศษ (Special Quasirandom Structure) ที่จำลองโครงสร้างช่วงคาบขนาดเล็ก โดยที่โครงสร้างแบบพิเศษนี้สามารถให้ผลการคำนวณคุณสมบัติเทียบเคียงกับโครงสร้างขนาดใหญ่ วิธีการที่เสนอนี้เป็นการเพิ่มประสิทธิภาพให้กับการจำลองโครงสร้างผลึก ด้วยการกำหนดค่าของตำแหน่งอะตอม A และ B โดยใช้หลัก Ising model แทนด้วยค่าสมมติสปินเสมือนกับชนิดอะตอมในแต่ละตำแหน่ง จากนั้นคำนวณค่าเฉลี่ยแต่ละตำแหน่งเพื่อนำมาสร้างเป็นโครงสร้างเสมือนสุ่มแบบพิเศษที่เป็นโครงสร้างช่วงคาบขนาดเล็ก ซึ่งจะนำโครงสร้างพิเศษนี้มาคำนวณคุณสมบัติทางไฟฟ้า โครงสร้างแถบช่องว่างพลังงาน รวมถึงคุณสมบัติทางอุณหพลศาสตร์ ในงานวิทยานิพนธ์นี้จะนำการจำลองโครงสร้างแบบพิเศษนี้นำมาใช้ร่วมกับทฤษฎีฟังก์ชันนัลของความหนาแน่น (Density Functional Theory) เพื่อศึกษาโครงสร้างอัลลอย สารประกอบโมลิดินัมทังสเตนไดซัลไฟด์ $Mo_{1-x}W_xS_2$ ชั้นเดียว ด้วยการจำลองโครงสร้างอัลลอยโดยใช้วิธีโครงสร้างเสมือนสุ่มแบบพิเศษ พบว่าจำนวนอะตอมในโครงสร้างคือ 27 ตัว ซึ่งมีขนาด 3x3x1 เซลล์ เหมาะสมในการคำนวณพลังงานและโครงสร้างแถบช่องว่างพลังงาน จากนั้นคำนวณโครงสร้างแถบช่องว่างพลังงาน ในงานวิทยานิพนธ์นี้พบว่า แถบช่องว่างพลังงานนั้นมีค่าแปรเปลี่ยนไปตามความเข้มข้นของทังสเตน นอกจากนี้เมื่อนำมาเทียบกับผลการทดลองในงานการทดลอง และงานจำลองด้วย Monte Carlo พบว่าได้ผลตรงกัน จึงสรุปได้ว่าการจำลองโครงสร้างอัลลอยโดยใช้วิธีโครงสร้างเสมือนสุ่มแบบพิเศษสามารถนำมาประยุกต์ใช้ได้กับการศึกษาโครงสร้างผลึกของสารประกอบอัลลอยได้เป็นอย่างดี

ภาควิชา	ฟิสิกส์	ลายมือชื่อนิสิต .....
สาขาวิชา	ฟิสิกส์	ลายมือชื่อ อ.ที่ปรึกษาหลัก .....
ปีการศึกษา	2559	ลายมือชื่อ อ.ที่ปรึกษาร่วม .....

5772150323 : MAJOR PHYSICS

KEYWORDS: SPECIAL QUASIRANDOM STRUCTURES / DENSITY FUNTIONAL THEORY / ALLOY MATERIALS / TRANSITION METAL DICHALCOGENIDE

WIRUNTI PUNGTRAKOON: MODEL OF MOLYBDENUM TUNGSTEN DISULFIDE ALLOY STRUCTURE USING SPECIAL QUASIRANDOM STRUCTURE METHOD. ADVISOR: ASST. PROF. THITI BOVORNRATANARAKS, CO-ADVISOR: ASSOC. PROF. UDOMSILP PINSOOK, 59 pp.

Substitutianal alloys are disorder crystalline structure. First-principles study of alloys is taken a large supercell that equivalent to a pure random structure. Structural models used in calculations of properties of substitutional random $A_{1-x}B_x$ alloys are usually constructed by randomly occupying each of the N sites of a periodic supercell by A or B. However, this method is not efficient. It is possible to design “Special Quasirandom Structures” (SQS) that simulate the small periodic supercell. It can be compared to structures that have large number of configurations or large cell sizes. The proposed method optimizes the supercell with the occupation of the atomic sites (A or B). This technique uses the language of Ising models to define the product of spin variable for each atomic site. Then calculate a lattice average to construct special periodic quasirandom structures. The SQS can be used in the calculation of optical and thermodynamic properties. This thesis uses the SQS method integrated with Density Functional Theory (DFT) to investigate alloy Molybdenum Tungsten Disulfide ($Mo_{1-x}W_xS_2$) monolayer. We found that SQS with 27 atoms to model 3x3x1 supercell structure is suitable for calculation of energy and band structure. Then the SQS of $Mo_{1-x}W_xS_2$ are studied by DFT calculations to evaluate band structures. We found tunability of band edges and band gaps by alteration of the W concentration. The results of the electronic structure studied by combination of DFT and SQS are in good agreement with experiment and Monte Carlo simulations from other works. We conclude that the model of alloy generated by SQS can be used to studies crystal structure behavior. This model uses low computational time but can achieve good result which agree well with the experiment report.

Department: Physics Student's Signature .....

Field of Study: Physics Advisor's Signature .....

Academic Year: 2016 Co-Advisor's Signature .....

ACKNOWLEDGEMENTS

This successful thesis comes from the cooperation of many people in ECPR laboratory. First of all, I gratefully thank my advisor, Assoc. Prof. Thiti Bovornratanaraks, for his support about introduction to interesting research topics and suggested research related. And deeply thank for useful advice to make this thesis completely. Also, I gratefully thank my co-advisor, Assoc. Prof. Udomsilp Pinsook, for useful advice about programing of SQS and suggestion on the GGA functional. Especially his always being encouragement, kindness and helpful towards me during research work. I would like to thank Asst. Prof. Rattachat Mongkolnavin, Dr. Rangsima Chanphana and Dr. Sornthep Vannarat for their time to examine my thesis. I want to thank financial support ⟦90⟧ ^th Year Chulalongkorn Scholarship from Graduate School, Chulalongkorn University. Finally, I profoundly thank all member of ECPR laboratory for their friendship and serviceable discussion on computational method and other research review.

CONTENTS

Page

Page

Page

LIST OF TABLES

Table page

LIST OF FIGURES

page

CHAPTER 1

Introduction

1.1 Computational modeling of solid state physics

The study conducted in solid state physics focuses on the states of matter formed by large numbers of strongly interacting atoms such as solids. For example, solution of many-body problem (e.g. Schrödinger equation in quantum mechanics) cannot be solved analytically. In such cases, numerical approximations are required. In computational activities, its execution of numerical analysis to solve problems. By using a quantitative theory already exists (e.g. Density Functional Theory for quantum model) [1]. This computational method is the subject that deals with these numerical approximations and then get results for matching up with experiment. In addition, the computational cost for many body problem tend to grow quickly. A macroscopic system typically has a size of the order of $\mathbf{10^{23}}$ constituent particles, so it is somewhat of a problem. Solving quantum mechanical problems is generally exponential growth of computational cost and time depend on the size of the system.

The computational modeling of solid state physics is said to be ab-initio or first principle calculation, followed by computations of the interactions of many number groups of atoms, until the bulk properties of the system had been determined. The Density Functional Theory (DFT) is a computational quantum mechanical modeling method used to investigate the electronic structure of many body systems. The electronical and physical properties of a system (many electron and ion system) can be determined by using functional. This case is the spatially dependent electron density. But there are still difficulties in using DFT to properly describe a complex system especially dopant interactions, transition states, strongly correlated systems with disorder stated, van der Waals forces and alloy interactions system.

By crystal structure prediction is the calculation of the crystal structures of solids from the first principles approach. With the DFT calculations on predicting the crystal structure of a compound based on its composition. The main goals of the computational modeling of solid state physics are to understand the properties of solid materials at the atomic level and predict both quantitative and theoretical data for the development of new materials.

1.2 Modeling of substitutional alloy disorder state

The main difference between a disorder state in single crystal alloy considered in ordinary ab-initio simulations and a real material is the inherent disorder. The most common form of disorder is the breakdown of the long-range order (LRO) of the crystal lattice sites. Most real solid materials have a hierarchy of structures beginning with atoms and ascending through various crystalline grains. The misoriented single crystals are separated by grain boundaries, interphase boundaries, etc. The only way to establish parameters of these polycrystalline systems is first derive data of microscopic nature and then transform these data to macroscopic quantities by suitable averaging methods based on statistical mechanics [2,3]. In the single crystals, the atomic disorder appears because of the random distribution of the atoms on the lattice sites. Substitution atoms on the single crystal components, it become randomly oriented and a disordered phase formed by randomly distributed atomic arrangements.

The most straightforward way to simulate disordered state in single crystal alloy use large unit cells (or supercells) with randomly distributed atoms on lattice. In principle, within the supercell approach one can consider both the local relaxation and short-range order (SRO) effects. However, because of the extremely large number of atoms needed for an arbitrary composition, this method is very intricate, and so far, mainly semi empirical and empirical methods have adopted it [4,5]. However, when supercells of random alloys are combined. The computational time grows exponentially with number of atoms in supercells. That is the hardest problem of the computational modeling, which depends on the computational cost and time.

For the substitutional alloys are designed by one metal substitutes for another in the structure. This case is called as binary or pseudo-binary alloys ($A_{1-x}B_x$ or $A_{1-x}B_xC$). By the substitutes metals must have similar atomic radius and bonding characteristics.

1.3 Two-dimensional materials Transition metal dichalcogenides (TMDC)

Since the isolation of graphene, a single-layer of graphite, in 2004. A large amount of research has been directed at isolating other two-dimensional (2D) materials due to their unusual characteristics and use in applications especially semiconductors [6]. The 2D materials, referred to single layer materials, are crystalline materials consisting of a single layer of atoms. But sometimes it refers to multiple layer materials. The multiple layers naturally form perfectly aligned stacks or layered combinations of different 2D materials. This feature can describe by van der Waals interaction between layers. While the first 2D material that has been discovered was graphene, then other 2D materials have been predicted to be stable and many remain to be synthesized with a significant challenge.

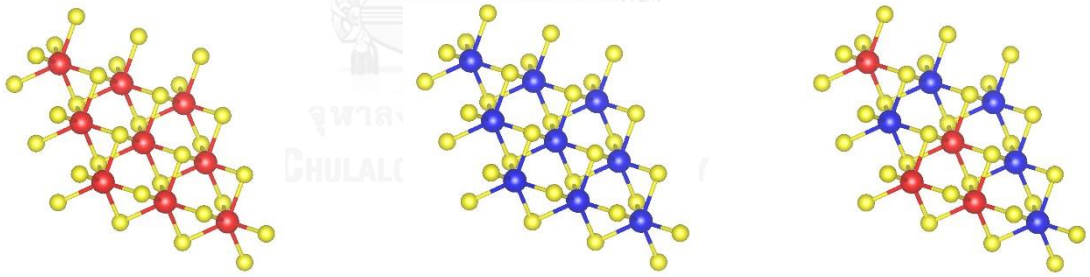

Figure 1.1 Substitutional pseudo-binary alloys model of structures, (left) is AC_2, (middle) is BC_2 and (right) shows substitutes by A into BC_2.

The 2D materials have attracted high interest from the research community. Graphene is the first example of such a 2D material. With its unique band structure in the limit of quantum confinement. This monolayer of carbon atoms has large number of applications in nanoelectronics and nanophotonics [7,8]. Recently, the research community has discovered a new family of 2D materials. That have unique band gap transition. Transition metal dichalcogenides (TMDC) have optical properties that can

construct to a semiconductor. A semiconductor can absorb photons with energy larger than or equal to its bandgap. If the minimum of the conduction band energy is at the same position in k-space as the maximum of the valence band called the direct band gap. Normally the band gap of bulk TMDC material down to a thickness multilayer is still indirect. Then separated TMDC to a monolayer the band gap now changes to direct [9]. The work on TMDC monolayers is an emerging research and development field since the discovery of the direct bandgap and the potential applications in electronics. The TMDC are often combined with other 2D materials like graphene and hexagonal boron nitride to make van der Waals heterostructure. These heterostructures need to be optimized to be possibly used as building blocks for a plenty of different devices such as transistors, solar cells, LEDs, photodetectors, fuel cells, photocatalytic and sensing devices. We will focus on crystal structure of TMDC later in Chapter 4. This section just to mention some information roughly for visualize about this works.

1.4 Outline

Chapter 1 is intended to provide a brief introduction of modeling crystal structures, disorder state and TMDC materials. The following Chapter 2 provides a fundamental knowledge of density functional theory, which is mainly used to investigate properties of crystal structures. An approach for modeling disorder state of crystal structures, alloy materials, by Special Quasirandom Structure (SQS) is given in Chapter 3. Chapter 4 shows methodology of modeling crystal structure by the first principle based on Quantum ESPRESSO program and use the Special Quasirandom Structure method to develop the monolayer molybdenum tungsten disulfide crystal structure. Chapter 5 shows the calculation electronical property the SQS of monolayer molybdenum tungsten disulfide. The last chapter, Chapter 6 reviews the results, obtained from the investigations in this thesis and about future works.

CHAPTER 2

DENSITY FUCTIONAL THEORY

2.1 Mathematical background of many-body problem

Quantum mechanics with the concept of wave-particle duality is used to describe the microscopic properties of condensed matters by solving the time dependent Schrödinger equation.

$$i\frac{\partial \Psi}{\partial t} = \hat{H}\Psi \tag{2.1}$$

where Ψ is the wave function containing all information of any system under consideration. Since all matter is composed of many microscopic particles, usually electrons and ions, interaction with each other, the Hamiltonian $\hat{H}$ of the system can be given by

$$\hat{H} = -\frac{1}{2}\sum_{i=1}^{n}\nabla_i^2 - \frac{1}{2}\sum_{I=1}^{N}\frac{1}{M_I}\nabla_I^2 - \sum_{i,I}\frac{Z_I}{|\boldsymbol{r_i} - \boldsymbol{R_I}|} + \frac{1}{2}\sum_{i\neq j}\frac{1}{|\boldsymbol{r_i} - \boldsymbol{r_j}|} + \frac{1}{2}\sum_{I\neq J}\frac{Z_I Z_J}{|\boldsymbol{R_I} - \boldsymbol{R_J}|}. \tag{2.2}$$

The first two terms in Eq. (2.2) are the kinetic energy of elections and ions respectively, where M_I denotes the mass of the ion at site I. Since both the ions and electrons are charged particles, the following three terms represent the potential energy due to the Coulomb interactions between electron & ion, electron & electron, and ion & ion. $\boldsymbol{r_i}$ is the electron position at site i, meanwhile $\boldsymbol{R_I}$ and Z_I are the position and the charge number of the ion at site I.

By solving Eq. (2.1) for a general system of condensed matters is impractical, since a macroscopic system consists of a number of particles in the order of Avogadro's number. The wave function that describing the system thus depends on a huge number of degrees of freedom, and can be expressed by

$$\Psi = \Psi(\boldsymbol{r_1}, \boldsymbol{r_2}, \dots, \boldsymbol{r_n}, \boldsymbol{R_1}, \boldsymbol{R_2}, \dots, \boldsymbol{R_N}, t). \tag{2.3}$$

To deal with difficulties problem, several approximations are involved in order to simplify the problem. Generally, the stationary ground state properties of the system are main interest. In this case, there is no explicit time dependence in the Hamiltonian. So, only the time independent Schrödinger equation should be significant to describe the system. The time independent Schrödinger equation can be written as

$$\widehat{H}\Psi = E_{tot}\Psi \tag{2.4}$$

so that, the wave function is change to time independent.

$$\Psi = \Psi(\boldsymbol{r_1}, \boldsymbol{r_2}, \dots, \boldsymbol{r_n}, \boldsymbol{R_1}, \boldsymbol{R_2}, \dots, \boldsymbol{R_N}) \tag{2.5}$$

A set of solutions for the eigenvalue equation Eq. (2.4), which represents the stationary states of $\widehat{H}$ with the corresponding total energy E_{tot}. Then we simplify the problem by Born-Oppenheimer approximation [10]. The approximation is based on the fact that the electrons are moving greatly faster than the ions because of their several orders of magnitude larger masses. At this point, we can assume that the ions are fixed form the electrons point of view. So, the kinetic term of the ions can be separated from Eq. (2.2) and also the ion & ion interaction term becomes a constant. The problem now reduces to the system of interaction electrons, meanwhile the electron & ion interaction term is treated as an external field acting on the electrons. So, the equation is reduced to the electron system can be written as

$$\widehat{H}_{elec}\Psi_{elec} = E_{elec}\Psi_{\mathbf{elec}} \tag{2.6}$$

now the problem reduces to the system of n-interacting electrons that can be describe by

$$\widehat{H}_{elec} = -\frac{1}{2}\sum_{i=1}^{n}\nabla_i^2 - \sum_{i,I}\frac{Z_I}{|\boldsymbol{r_i} - \boldsymbol{R_I}|} + \frac{1}{2}\sum_{i\neq j}\frac{1}{|\boldsymbol{r_i} - \boldsymbol{r_j}|} \tag{2.7}$$

$$\Psi_{elec} = \Psi_{elec}(\boldsymbol{r_1}, \boldsymbol{r_2}, \dots, \boldsymbol{r_n}) \tag{2.8}$$

the eigenvalues E_{elec} represents the corresponding energies of the electronic system. So, the total energy E_{tot} of the system in Eq. (2.4) can thus be easily compute from

$$E_{tot} = E_{elec} + E_{ions}\,, \tag{2.9}$$

where E_{ions} is constant; $E_{ions} = -\frac{1}{2}\sum_{I=1}^{N}\frac{1}{M_I}\nabla_I^2 + \frac{1}{2}\sum_{I\neq J}\frac{Z_I Z_J}{|\boldsymbol{R_I} - \boldsymbol{R_J}|}$.

The problem can be further simplified if the system under consideration is periodic, e.g. crystalline solids. Demonstrated by Bloch [11] that, due to the periodicity of the

crystal, it is sufficient to consider only the primitive unit cell consisting of a few particles, rather than taking into account a large number of particles in the macroscopic crystal. In this case, the wave function Ψ_{elec} are taking the form

$$\Psi_{elec} = \psi_{nk(\boldsymbol{r})} = e^{i\boldsymbol{k}\cdot\boldsymbol{r}} u_{nk(\boldsymbol{r})}\,, \tag{2.10}$$

where $\boldsymbol{n}$ is the band index and takes number $n = 1, 2, 3, \ldots$ and $\boldsymbol{k}$ is a reciprocal vector, principally in the first Brillouin zone, $u_{nk(\boldsymbol{r})}$ is a function with periodicity of the crystal lattice and $e^{i\boldsymbol{k}\cdot\boldsymbol{r}}$ describes a plane wave.

Even though the problem is much simplified through the above approximation, it is still insufficient to directly solve Eq. (2.6). This is because solving the Schrödinger equation for a system containing more than a few particles is in fact practically formidable.

2.2 The Hohenberg-Kohn theorems

Instead of solving for the many electron wave function Ψ_{elec}, one preferably uses the electron density $n(\boldsymbol{r})$ as a basic variable. For a system of n-interacting electrons which is described by electron density so the number of spatial coordinates reduces from $3n$ to 3, thus substantially simplify the problem. Hohenberg and Kohn formulated two theorems [12], based on $n(\boldsymbol{r})$ that has been seen at the starting point of modern density functional theory (DFT). The two theorems are stated as follows

Theorem I; For any system of interaction particles in an external potential $V_{ext}(\boldsymbol{r})$, the potential $V_{ext}(\boldsymbol{r})$ is determined uniquely, except for a constant, by the ground state particle density $n_0(\boldsymbol{r})$.

Theorem II; A universal function for the energy $E[n]$ in term of the density $n(\boldsymbol{r})$ can be defined, valid for any external potential $V_{ext}(\boldsymbol{r})$. For any particular $V_{ext}(\boldsymbol{r})$, the exact ground state energy of the system is the global minimum value of this functional, and the density $n(\boldsymbol{r})$ that minimizes the functional is the exact ground state density $n_0(\boldsymbol{r})$.

The two theorems are clear that if the total energy functional $E[n]$ was known, all the ground state properties of any electronic system could be exactly determined by the ground state density $n_0(\boldsymbol{r})$. The total energy functional can be expressed

$$E[n] = T[n] + E_{int}[n] + \int V_{ext}(\boldsymbol{r}) n(\boldsymbol{r}) d^3r + E_{ions}\,, \tag{2.11}$$

where the first term is the kinetic energy of the interacting electrons, meanwhile the following three terms represent the potential energies due to the Coulomb interaction between the electrons, the Coulomb interaction of the electron density $n(\boldsymbol{r})$ with the external field $V_{ext}(\boldsymbol{r})$, and the interaction between the ions respectively. However, the problem now reduces from solve for the system of n-interacting electrons to solve the exact forms of $T[n]$ and $E_{int}[n]$.

2.3 Kohn-Sham equations

Main idea is to replace the real system of interacting many-particle by an artificial system of non-interacting particles. The idea was proposed a practical approach by Kohn and Sham [13] to overcome the difficulties in solving for the ground state properties of the interacting many-particle problem. The density $n(\boldsymbol{r})$ is the real one. Rather than the external potential $V_{ext}(\boldsymbol{r})$, each non-interacting particle is subjected to the effective potential $V_{eff}(\boldsymbol{r})$, given by

$$V_{eff}(\boldsymbol{r}) = V_{ext}(\boldsymbol{r}) + \int \frac{n(\boldsymbol{r}')}{|\boldsymbol{r} - \boldsymbol{r}'|} d\boldsymbol{r}' + V_{xc}(\boldsymbol{r}) \,. \tag{2.12}$$

The second term in Eq. (2.12) is the Coulomb interaction between the electrons, that is called Hartree potential. The term $V_{xc}(\boldsymbol{r})$ is defined as the exchange correlation potential, accounting all the quantum many-particle interactions and can be calculated from the exchange-correlation energy functional $E_{xc}[n(\boldsymbol{r})]$ by

$$V_{xc}(\boldsymbol{r}) = \frac{\partial E_{xc}[n(\boldsymbol{r})]}{\partial n(\boldsymbol{r})} \,. \tag{2.13}$$

Therefore, the non-interacting particles can be described by the Kohn-Sham wave functions ψ_i, which are the eigenstates of the single particle, of Schrödinger like equation.

$$\left(-\frac{1}{2}\nabla^2 + V_{eff}(\boldsymbol{r})\right)\psi_i(\boldsymbol{r}) = \epsilon_i \psi_i(\boldsymbol{r}) \,. \tag{2.14}$$

This equation is called as Kohn-Sham equation. Where ϵ_i is the eigenvalue of the non-interacting single particle, corresponding to the Kohn-Sham eigenstate ψ_i. By under the Kohn-Sham scheme, the particle density $n(\boldsymbol{r})$ of a system with N noninteracting particles can be easily obtained as

$$n(\boldsymbol{r}) = \sum_{i=1}^{N} |\psi_i(\boldsymbol{r})|^2 \ . \tag{2.15}$$

The Kohn-Sham total energy functional is given by

$$E_{KS}[n] = T_s[n] + \int V_{ext}(\boldsymbol{r}) n(\boldsymbol{r}) d^3r + E_{Hartree}[n] + E_{xc}[n] + E_{ions} \ , \tag{2.16}$$

where $T_s[n]$ is the kinetic energy functional of the non-interacting particles express by

$$T_s[n] = -\frac{1}{2} \sum_{i=1}^{N} \langle \psi_i | \nabla^2 | \psi_i \rangle \tag{2.17}$$

and $E_{Hartree}[n]$ is the classical Coulomb energy functional due to a particle density $n(\boldsymbol{r})$, with self-interacting. The expression of the $E_{Hartree}[n]$ functional is given by

$$E_{Hartree}[n] = \frac{1}{2} \int \frac{n(\boldsymbol{r}) n(\boldsymbol{r}')}{|\boldsymbol{r} - \boldsymbol{r}'|} d\boldsymbol{r} d\boldsymbol{r}' \ . \tag{2.18}$$

2.4 Exchange correlation functional

Although the problem is changed to non-interaction system, but the major problem to solve the Kohn-Sham equation Eq. (2.14) is that the form of the exchange correlation functional $E_{xc}[n]$ is not solved exactly. However, it is still possible to formulate the functional with some approximations. Many way approaches to estimate $E_{xc}[n]$ have been proposed and constantly developed to improve the accuracy compare with experiments. The most approaches are extensive used for approximations, that are given as follows;

Local density approximation (LDA)

The local density approximation (LDA) is the simplest way to derive $E_{xc}[n]$. LDA was first suggested in 1965 [13]. In practice, LDA approximates $E_{xc}[n]$ by assuming that the exchange correlation energy density at each point $\boldsymbol{r}$ in space is in the same form as the homogeneous electron gas $\epsilon_{xc}^{\text{hom}}(n(\boldsymbol{r}))$, which has been well studied using quantum Monte Carlo simulations [14]. The expression of $E_{xc}^{LDA}[n]$ is thus given by

$$E_{xc}^{LDA}[n] = \int n(\boldsymbol{r}) \epsilon_{xc}^{hom}\big(n(\boldsymbol{r})\big) d\boldsymbol{r} \, . \tag{2.19}$$

Unfortunately, LDA was supposed to work well only for system with slowly varying density. However, it was found to be successful also for systems with high density

gradient. The explanations to the relative success of LDA have been described elsewhere [15, 16].

Generalized gradient approximation (GGA)

GGA was improve the accuracy by considering not only the density $\boldsymbol{n(r)}$ but also the gradient of the density at the same point $\boldsymbol{r}$ to approximate $E_{xc}[n]$, were proposed [17-19] as an extension of LDA. Therefore,

$$E_{xc}^{GGA}[n] = \int n(\boldsymbol{r})\epsilon_{xc}^{GGA}\big(n(\boldsymbol{r}), \nabla n(\boldsymbol{r})\big)d\boldsymbol{r}\,. \qquad (2.20)$$

The calculations in this thesis were performed using GGA in the form of Perdew, Burke, and Ernzerhof (PBE) [19], as implemented in the Quantum ESPRESSO package [20].

2.5 Plane-wave basis sets

Explanation solve the Kohn-Sham equations in Eq. (2.14) by numerical method. The electron wave functions $\boldsymbol{\psi_i(r)}$ need to be expanded in a basis set. Different choices of basis sets are available, e.g. Gaussians, plane-waves and atomic orbitals. According to the Bloch's theorem [11], the plane-wave is considered as the first choice among the others, as he demonstrated that the wave functions of systems with periodicity can in principle be expanded in term of a plane-wave basis set likes Eq. (2.10). Practically, the basis set needs to be truncated at a finite cutoff energy. Based on the characteristic of the electron wave functions, it may be splitting in space into an interstitial and core region. In the interstitial region between atoms, the valence electrons, the wave function is rather smooth and only a small number of plane-waves is already sufficient to well reproduce the wave function. In addition, a large number of plane-waves with very high energy cutoff is required to accurately represent the oscillating wave function inside the core region due to the strong Coulomb interactions between the localized core electrons and the nucleus, so resulting in an extremely high computational cost.

To implement the plane-wave basis sets practically, one employs a pseudopotential approach, that was suggested by Hellmann [21, 22]. The pseudopotential approach substitutes the real Coulomb potential by a smooth effective potential, specially designed in order to smoothen the rapidly oscillating part

of the wave function within a pseudo wave function, thus substantially reducing both the basis sets (imply to the computational demand). Inspired by the fact that only the valence electrons in the interstitial region are taking part in the bonding formation, elimination of the oscillating part within the core region thus should not be affecting the bonding properties. Within the pseudopotential approach, the pseudo wave function is determined by a certain cutoff radius from the nucleus. A few criteria to construct the pseudopotential is given by the pseudopotential need to reproduce the scattering properties of the core region. And outside the cutoff radius, the behavior of the pseudopotential and the pseudo wave function must be the same to the real ones. Among numerously developed versions of the pseudopotentials suggested in the literature, Norm-conserving [23] and Ultrasoft [24] pseudopotentials are most used in plane-wave basis set based on DFT calculations.

2.6 Solving the Kohn-Sham equations

The ground state density $\boldsymbol{n_0(r)}$ is searched by minimizing the Kohn-Sham total energy functional in Eq. (2.16). The Kohn-sham equations Eq. (2.14) must be solved self-consistently. Since the effective potential $\boldsymbol{V_{eff}}$ and the Kohn-Sham orbitals $\boldsymbol{\psi_i}$ in Eq. (2.14) are determined by the density $\boldsymbol{n(r)}$, which is not known yet, several iterative cycles of solving the Kohn-Sham equations must be performed as self-consistently calculations by guess density (illustrated in Fig.2.1). The first step to solve the equation is to guess the initial density $\boldsymbol{n_{initial}(r)}$ in order to construct $\boldsymbol{V_{eff}}$, according to Eq. (2.12). After solving the Kohn-Sham equations one obtains a set of $\boldsymbol{\psi_i}$, which is in turn used to calculate a new density $\boldsymbol{\tilde{n}_{k+1}(r)}$. If the convergence criterion is not fulfilled, $\boldsymbol{\tilde{n}_{k+1}(r)}$ will be mixed with the input density $\boldsymbol{n_k(r)}$ using different numerical mixing schemes to get $\boldsymbol{n_{k+1}(r)}$ as a new input to construct a new $\boldsymbol{V_{eff}}$, and then another iterative cycle of solving Kohn-Sham equation is performed. Such a process continues until the density converges and self-consistency is thus reached.

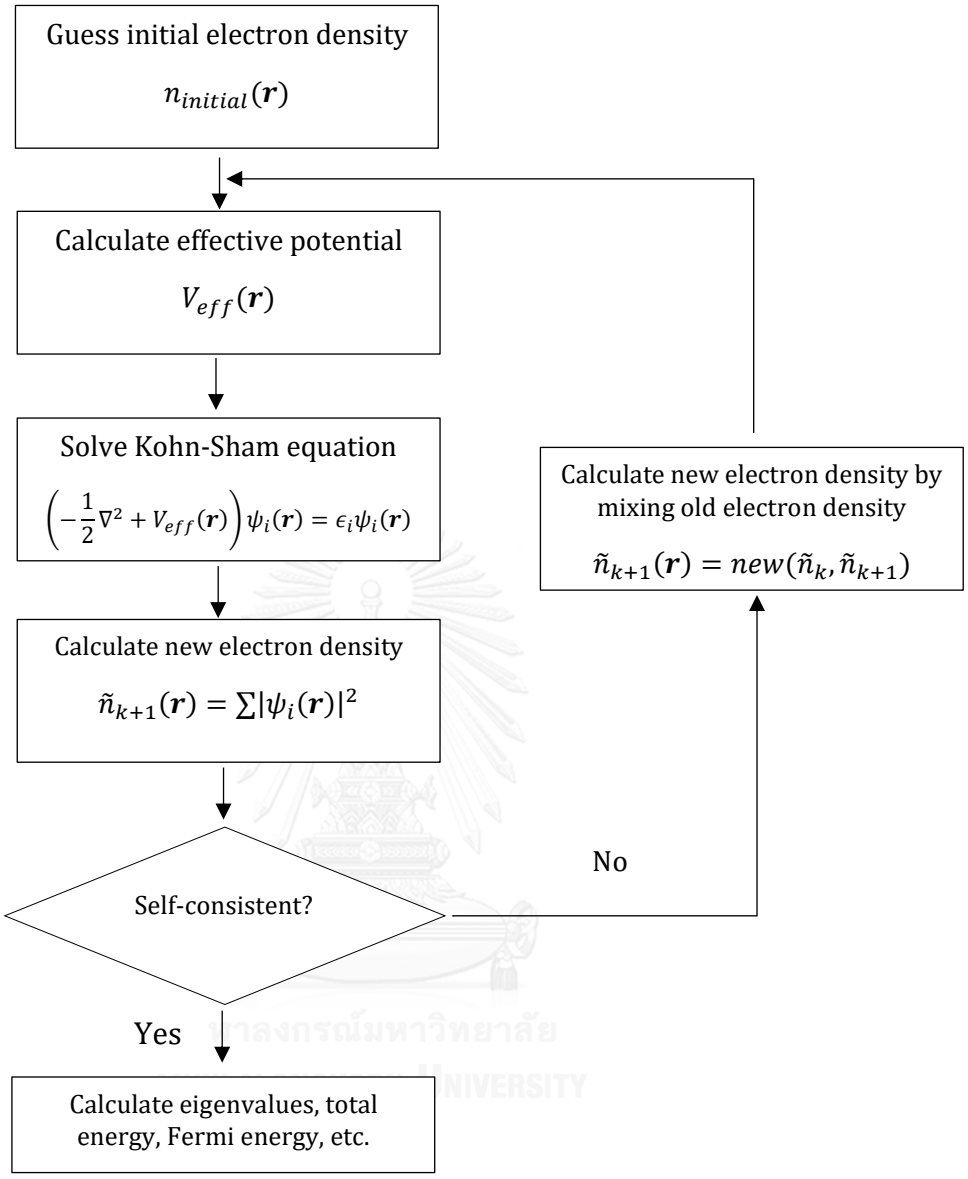

Figure 2.1 Flowchart of the self-consistent loop for solving Kohn-Sham equations.

CHAPTER 3

MODELING ALLOY MATERIALS BY SPECIAL QUASIRANDOM STRUCTURE METHOD

3.1 Primitive unit cell to supercell approach

The Bloch's theorem [11], that suggests alternative way to dealing with many particles in the macroscopic crystal, allows one to consider only a small primitive unit cell consisting of a few particles due to the periodicity in the crystal. However, considering effects of configurational disorder in modeling substitutionally disordered alloys, for example alloying material destroys the periodicity in the crystal, thus the Bloch's theorem is no longer valid. In this case, one can implement a supercell approach, consist of several primitive unit cells depend on the supercell's size. That can introduce different degrees of configurational disorder state. The periodicity of the introduced configurational disorder is represented by the supercell.

3.2 Structural theories of alloys

3.2.1 Direct sampling methods

A binary $A_{1-x}B_x$ substitutional alloy with a lattice of N sites can occur in 2^N possible atomic arrangements, denoted as "configurations" σ. Each configuration exhibits certain physical properties (e.g., total energy, band gap, etc.) denoted symbolically by $E(\sigma)$. The measurable property $\langle E \rangle$ represents an ensemble average over all 2^N configurations σ

$$\langle E \rangle = \sum_{\sigma}^{2^N} \rho(\sigma) E(\sigma), \tag{3.1}$$

where the density matrix $\rho(\sigma)$ denotes the probability to find configuration σ in an ensemble of systems. The obvious difficulty with structural theories of alloys based

on Eq. (3.1) lies in the need to relax, then average over many configurations. In practice, one proceeds by either (1) selecting a smaller number of representative configurations, such as in the Monte Carlo method [25], or by (2) using a single, sufficiently large configuration. While by the principle of spatial ergodicity, all possible finite environments are realized in a single, $N \to \infty$ sample, in practice far smaller supercells have been used. The first example utilized highly simplified Hamiltonians, current first-principle with classical model, self-consistent theories of the electronical degrees of freedom are restricted to $N \lesssim 50$ atoms [26]. This direct sampling approach explicitly specifies the alloy structure, and can hence incorporate atomic relaxations. However, it approaches the statistical limit as slowly as $N^{-1/2}$. Therefore, it involves a rather large number of different configurations or large cell sizes. That make self-consistent theories are still impractical.

3.2.2 Mathematical model of cluster expansions

Rather than address directly the property $E(\sigma)$ of configuration σ. In order to account for a contribution of configurational disorder in any crystalline material. It is necessary to understand the concept of cluster expansion of the configurational part of the total energy for a given alloy, as developed by Sanchez, Ducastelle, and Gratias for multicomponent alloy systems [27]. In this section, a brief introduction to the concept of cluster expansion will be given, based on the review article by Ruban and Abrikosov [28].

For simplicity, one considers a binary alloy, $A_{1-x}B_x$. The atomic configuration of the alloy, $A_{1-x}B_x$, is described by pseudo spin variables σ_i, where σ_i takes the values $+1, (-1)$ if site i is occupied by A, (B) type atom, respectively. For an alloy system, consisting of N atomic sites, the atomic configuration of that alloy can be specified by the vector $\boldsymbol{\sigma} = \{\sigma_1, \sigma_2, \sigma_3, \dots, \sigma_N\}$. The product of spin variables σ_i in turn determines a basis function for a given n-site cluster f (call as figures). The figure is defined by the number k of atoms located on its vertices ($k = 1,2$ are sites, pairs), the order m of neighbor distances separating them ($m = 1,2$ are first, second neighbors, etc.), thus the figures can define by the number k and m ($f \equiv (k, m)$). By using the language of Ising models, then $\Phi_f^{(n)}(\boldsymbol{\sigma})$ given by

$$\Phi_f^{(n)}(\boldsymbol{\sigma}) = \prod_{i \in f} \sigma_i \,. \tag{3.2}$$

These functions form a complete and orthonormal set with the inner product between two functions, given by

$$\left\langle \Phi_f^{(n)}(\boldsymbol{\sigma}), \Phi_g^{(n)}(\boldsymbol{\sigma}) \right\rangle = \frac{1}{2^n} \sum_{\boldsymbol{\sigma}} \Phi_f^{(n)}(\boldsymbol{\sigma}) \Phi_g^{(n)}(\boldsymbol{\sigma}) = \delta_{f,g} \,. \tag{3.3}$$

The sum in Eq. (3.3) runs over all atomic configuration $\boldsymbol{\sigma}$, and $\delta_{f,g}$ is the Kronecker's delta. The scalar product, obtained from Eq. (3.3), is thus equal to 1 only if $\Phi_f^{(n)}(\boldsymbol{\sigma})$ and $\Phi_g^{(n)}(\boldsymbol{\sigma})$ are specifying the exactly same n-site clusters in the crystal, while the product of any two clusters with different numbers of atoms is always equal to 0.

As the basis set is complete and orthonormal, one can expand any alloy's property $E(\boldsymbol{\sigma})$, which is a function of the configuration in this basis set

$$E(\boldsymbol{\sigma}) = \sum_f \epsilon_f^{(n)} \Phi_f^{(n)}(\boldsymbol{\sigma}) \tag{3.4}$$

The discretization of a configuration into a hierarchy of figures affords a corresponding hierarchy of approximations for measurable properties, for example the ensemble average over configurations. In Eq. (3.4) $\epsilon_f^{(n)}$ denotes the contribution of figure f at n-sites cluster to a physical property E for configuration $\boldsymbol{\sigma}$ ($E(\boldsymbol{\sigma})$, where the sum is running over all clusters in the considered alloy system. The expansion coefficients $\epsilon_f^{(n)}$, call as effective cluster property is given by the projections Eq. (3.3) on the Eq. (3.4) as

$$\epsilon_f^{(n)} = \frac{1}{2^n} \sum_{\boldsymbol{\sigma}} E(\boldsymbol{\sigma}) \Phi_f^{(n)}(\boldsymbol{\sigma}) \,. \tag{3.5}$$

Since $E(\boldsymbol{\sigma})$ depends on composition, ϵ_f does too.

Note that $\epsilon_f^{(n)}$ does not depend on n-sites cluster, since Eq. (3.5) indicates that $\epsilon_f \equiv \epsilon_f^{(n)}$ has full symmetry of the crystal. Using Eq. (3.2), the cluster expansion of Eq. (3.4) can be written as

$$E(\boldsymbol{\sigma}) = \sum_f \prod_{i \in f} \sigma_i \, \epsilon_f \,. \tag{3.6}$$

So, the ensemble average of the physical property E is

$$\langle E \rangle = \sum_f \left\langle \prod\nolimits_{i \in f} \sigma_i \right\rangle \epsilon_f \,. \tag{3.7}$$

The basic problem of a direct sampling of $E(\boldsymbol{\sigma})$ over 2^N terms (Eq. (3.1)) is reduced to sum over specific n-sites cluster. Where one needs to calculate the effective cluster properties ϵ_f and sum over all types of figures f. Note that the expansions in Eq. (3.2) – Eq. (3.7) are rigorous as long as the sum is not truncated. For a perfectly random infinite alloy (denote configuration $\boldsymbol{\sigma}$ as R), the correlation functions are known in advance [29]. They are

$$\prod_f R = \prod_{k,m} R = \left\langle \prod_{k,m} R \right\rangle = (2x-1)^k \,, \tag{3.8}$$

where f has been replaced by the equivalent indices (k,m). For example, at $x = \frac{1}{2}$, the correlation function of configuration perfectly random vanish to all orders, except $f = (k,m) = (0,1)$ the correlation function equal 1. So, the ensemble average of physical property E can easy compute by

$$\langle E \rangle_R = \sum_{k,m} (2x-1)^k \epsilon_{k,m} \,. \tag{3.9}$$

Now, the ensemble average of physical property E is calculated by summation of the effective cluster properties weight by the correlation functions for each figure. Practical application of lattice models assumes that the cluster expansion of Eq. (3.9) for the physical property E is rapidly convergent, so that only a few terms need to be kept. Therefore, only a few of the effective cluster properties for each figure must be knowns. By under this assumption, we can find a method that utilize for modeling alloy materials. That method suggested by Zunger et al. [30] is called as the Special Quasirandom Structure (SQS). In the case of completely random alloys (as Eq. (3.9)), they are practically often defined by The Warren-Cowley short range order (SRO) parameters that represent the 2-site correlation functions ($k = 2$) [28]. For a binary alloy, $A_{1-x}B_x$, the SQS approach constructs a supercell by distributing A and B atoms in a way that the SRO parameters between both kinds of atoms are zero, or close to zero for as many coordination shells as possible with focus on the short-range shells to mimic the configuration. The next sections will describe the SQS approach idea and provides an unbiased starting point for modeling random substitutionally disordered alloys.

3.3 Special Quasirandom Structure

3.3.1 The idea of the SQS approach

Instead of attempting to approach cluster expansion by calculate the random correlation functions ($\epsilon_{k,m}$). We will instead design a N-atom periodic supercell structure (a special configuration structure), whose distinct correlation functions best match the ensemble average of the random alloy in Eq. (3.8). The cluster expansion in previous section shows that the amount by which the physical property $E(\boldsymbol{\sigma} = S)$ of a given structure s fails to reproduce the ensemble average $\langle E \rangle$ of the perfectly random alloy can be represented in terms of a hierarchy of figures. By combine Eq. (3.6) and Eq. (3.9),

$$\langle E \rangle_R - E(S) = \sum_{k,m} \left[(2x-1)^k - \prod_{k,m} S \right] \epsilon_{k,m} \ . \tag{3.10}$$

From Eq. (3.10), it obviously can be concluded that, we model the special configuration structure S based on the results of the correlation functions $\prod_{k,m} S$. If the special configuration structure S is designed by looking cases to obtain zero value of Eq. (3.10). Its means that the physical property of the special configuration structure $E(S)$ is equal to the ensemble average of the perfectly random alloy $\langle E \rangle_R$, then the special configuration structure S can be used instead for any calculation physical properties (e.g., total energy, band gap, etc.). In addition, we do not necessary calculate the effective cluster property $\epsilon_{k,m}$, reduce computational cost and time for calculation physical properties.

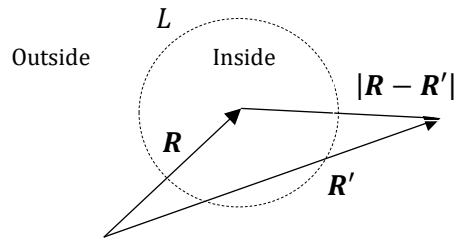

Figure 3.1 The characteristic length scale L of property E, that use for scaling size of figure. Indicate value of (k, m) sufficient for the disordered system studied.

Especially problem of modeling alloy method now is changed to find a structure that has correlation function value close to a disordered system we investigate or are

interested. In turn, the contribution $\epsilon_{k,m}$ to the property $\boldsymbol{E}$ is expected to fall off with size of figure. Indeed, in disordered systems the physical characteristic $\boldsymbol{E}$ at point $\boldsymbol{R}$ depends primarily on the environment inside a neighborhood $|\boldsymbol{R}-\boldsymbol{R}'| < L$ (the effect of more distant neighbors falls off exponentially with $|\boldsymbol{R}-\boldsymbol{R}'|/L$), where $\boldsymbol{L}$ is a characteristic length scale of property $\boldsymbol{E}$. It is hence natural to select the occupations by $\boldsymbol{A}$ and $\boldsymbol{B}$ for the special configuration structures $\boldsymbol{S}$ so that Eq. (3.10) is minimized in a hierarchical manner.

3.3.2 Programing of SQS

The previous section shows the basic idea of SQS approach thats represent how to model alloy materials by using cluster expansion, and then with some approximation of perfectly random alloy. Now we will design a $\boldsymbol{N}$-atom periodic supercell structure, whose distinct correlation functions best match the ensemble average of the random alloy in Eq. (3.10). And the result of the characteristic length scale that forces the property $\boldsymbol{E}$ is expected to fall off with size of figure. From those requirements that are mentioned above. The expectation for modeling alloy materials are used by computation programing, which is how to program to follow the idea of SQS approach with many conditions that match on any disorder systems. According to the first step of modeling materials, the first thing that we need is a primitive cell structure (a cell parameter and atomic positions). That information obviously infers that cell is a periodic cell. The information (cell parameters and atomic positions), which have been inputted into the program, be converted to a new one that represent a large number of atoms in the macroscopic crystals.

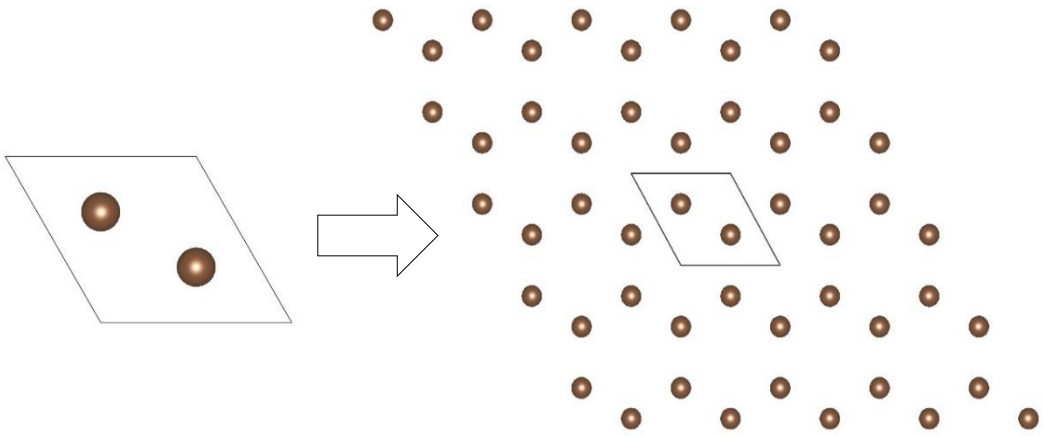

Input Storing information on program

Figure 3.2 An idea for the input information converted to the storing information on program by multiple the cell structure.

Form the previous section, the figure determines by scale of multiple the cell structure, if we need a huge figure then multiple the cell structure three or four time. It depends on the size of input cell structure and the neighbors atomic distance. In fact, the pair correlation functions with spanning distance up to the ninth atomic neighbor shells shall be sufficient for many pseudo-binary alloy materials (by result of characteristic length scale). In Figure 3.3 describe a relevance about the figure (k, m) where k is the number of vertices in the figures and the m is the distance order of the nearest neighbors.

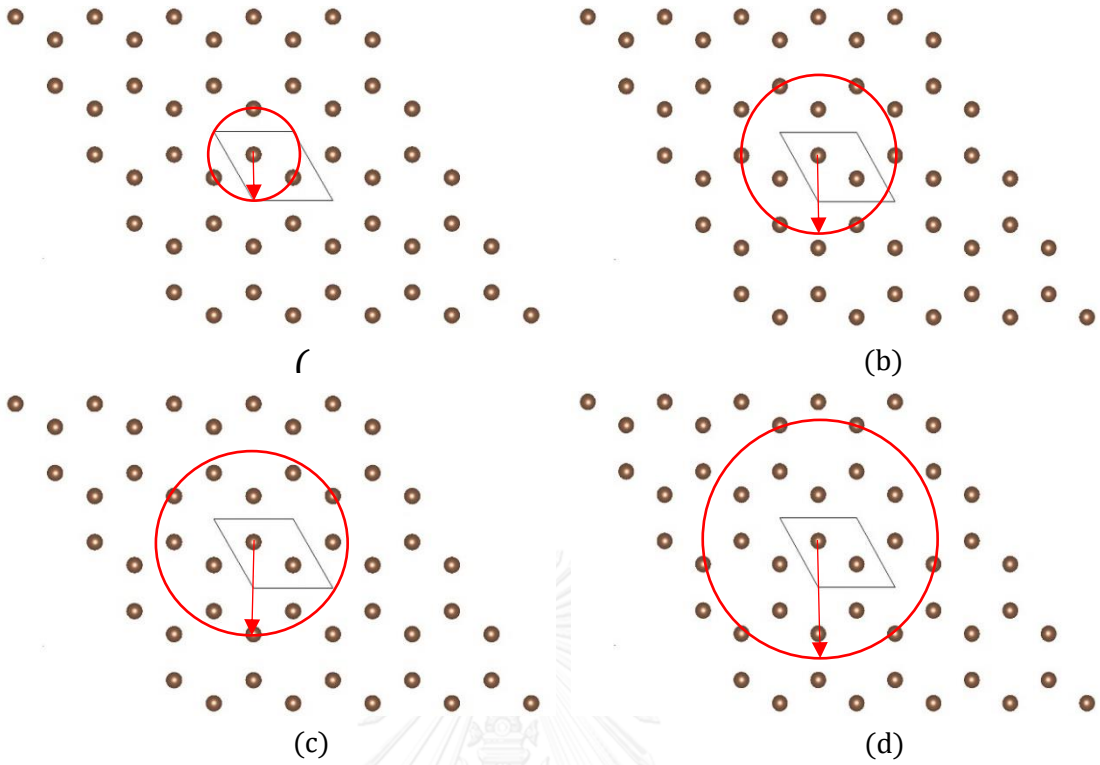

Figure 3.3 Example of the pair figure ($k = 2$) for (a) the first nearest atomic neighbor ($m = 1$, first shell), (b) the second nearest atomic neighbor ($m = 2$, second shell), (c) the third nearest atomic neighbor ($m = 3$, third shell), (d) the fourth nearest atomic neighbor ($m = 4$, fourth shell). For each shell in this diagram shows the number of nearest atomic neighbor are 3, 6, 3 and 6 respectively.

The example of the pair figure (in Figure 3.3) shows that if we need to span distance up to the ninth atomic neighbor shells some information (the number of nearest atomic neighbor at some shells) may be lost. Because the program multiple the cell structure (two atoms per cell) too little to apply for the pair figure up to the ninth atomic neighbor. As mentioned above the program must manage storing information of atomic position to appropriate the disorder system being studied.

The second step of programing, modeling alloy materials (binary or pseudo-binary alloy $A_{1-x}B_x$), assign a pseudo-spin S_i = -1 (+1) to each occupation site, if $A(B)$ atom occupies at site i. This configuration depends on the disorder system being studied, which are the number of atoms and the concentration of the substitutional atoms (x compositions). For this action in the second step of programing is simply to

compute. Now taking the product of the pseudo-spin variables over all the sites of the figures and then averaging over all symmetry equivalent figures of the lattice. The result of this compute is what we need, the correlation functions $\prod_{k,m} \boldsymbol{S}$ of the interested figure. A diagram of assign a pseudo-spin and compute the product of the pseudo-spin here in Figure 3.4

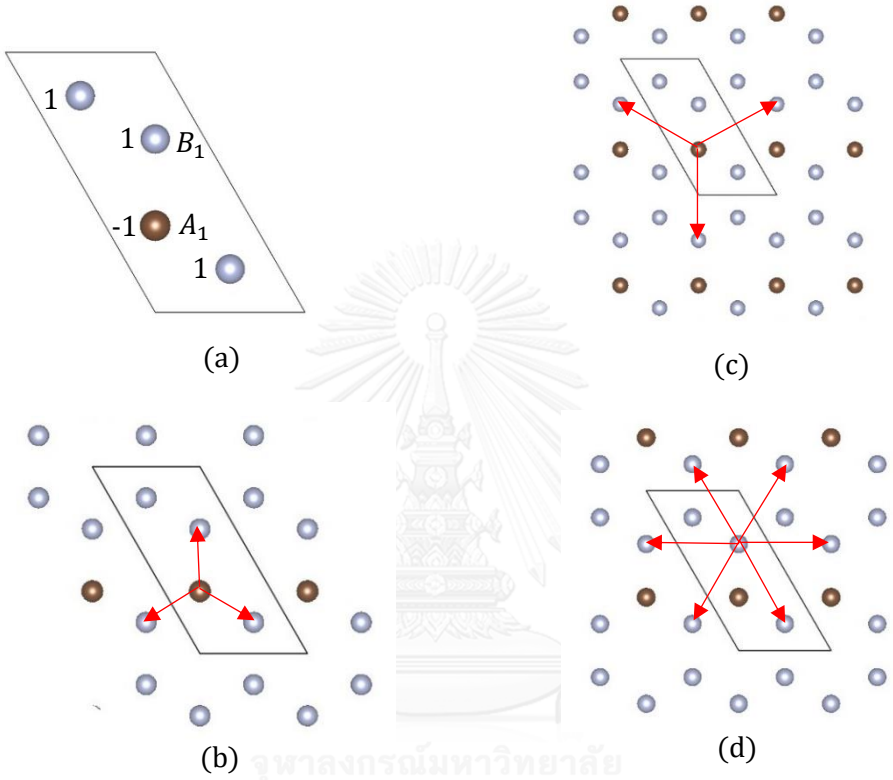

Figure 3.4 Example lattice cell contain 4 atoms. (a) assign pseudo-spin on all atoms in the lattice A_1B_3 atom A, B is -1, 1 then consider at site A_1 and B_1 (b) compute correlation function $(k = 2, m = 1)$ at site A_1 (c) compute correlation function $(k = 2, m = 3)$ at site A_1(d) compute correlation function $(k = 2, m = 2)$ at site B_1.

The correlation functions for each site are calculated by $\prod_{k,m} \boldsymbol{S}$. The Figure 3.4(b) value of the correlation functions depends on type of pseudo-spin. Each occupation sites on the figure (2,1) at site A_1, which is computed by

$$\left(\prod_{2,1} \boldsymbol{S}\right)_{A_1} = \frac{[(-1*1)+(-1*1)+(-1*1)]}{3} = -1\,. \qquad (3.11)$$

Now from this example lattice cell A_1B_3, the averaging over all symmetry figures (2,1) consist of 4-sites (A_1, B_1, B_2, B_3) be obviously calculated by

$$\overline{\prod_{2,1} \boldsymbol{S}} = \frac{\left[-1 + \frac{1}{3} + 1 - \frac{1}{3}\right]}{4} = 0\,, \tag{3.12}$$

and value of the ensemble average of the correlation functions A_1B_3 equal 0.25 (compute by $(2x-1)^2, x = 3/4$). From the calculation above means the correlation function $\prod_{2,1} \boldsymbol{S}$ of this lattice doesn't match on perfectly random by comparison. In this section, the program should be calculating the correlation functions up to the ninth atomic neighbor for each site on the lattice studied. Then take the result into consideration, that is the best periodic supercell approximation to the perfectly random state for a given number of atoms per supercell.

In fact, although it can be programed to calculate the correlation functions and approximation to the perfectly random. But how the program can find or predict "the best periodic supercell", which is really need for study alloy materials. Because modeling alloy materials by SQS method does not need to calculate any physical property so, we do a brute force method. The last step performs by looping the second step with every configuration atomic arrangement for a given number of atoms per supercell. And then compare every result from the second step for choosing the best periodic supercell, which is used by DFT calculation to studies behavior of physical and electronical property (likes the formation enthalpies, density of states, optical properties, and band gaps) see also Appendix C. The concept of the SQS method to overcome the prohibitive computational cost associated with directly constructing a large supercell with random occupancies of large number of atoms. The SQS is designed for a rather small periodic supercell that concept as follows.

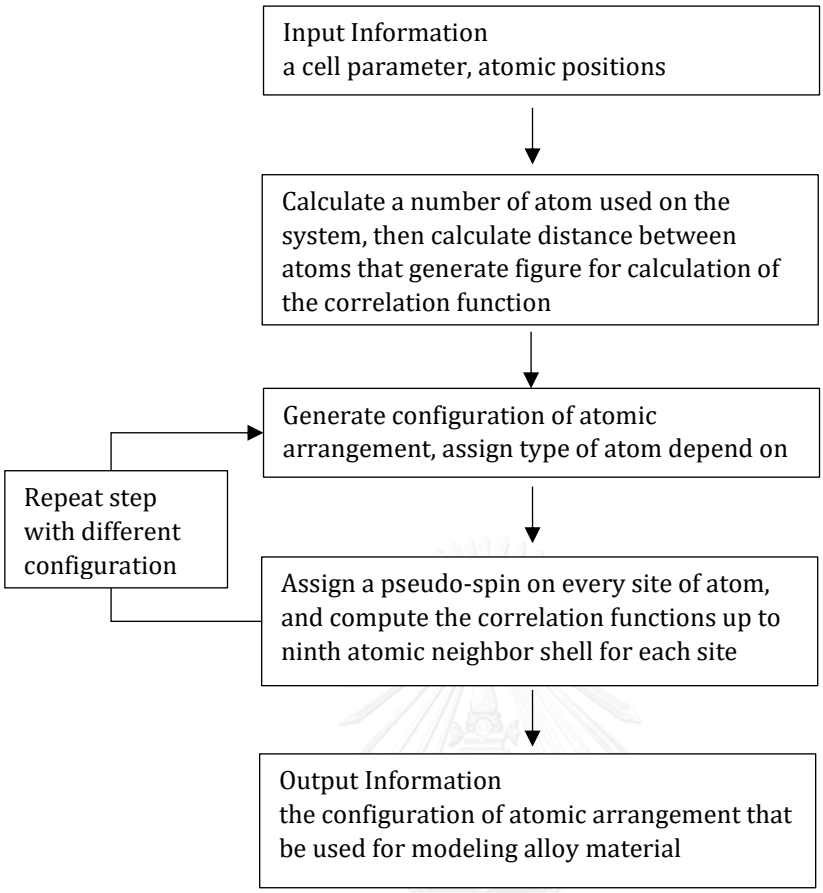

Figure 3.5 Flowchart of the basic idea for programing of Special Quasirandom Structure method.

CHAPTER 4

STUDY OF ALLOY MOLYBDENUM TUNGSTEN DISULFIDE ($Mo_{1-x}W_xS_2$) 2D MATERIAL

4.1 Ab-initio study of MoS_2 and WS_2 monolayers

Transition metal dichalcogenides (TMDC) are a class of a material with the composition MX_2 , where M denotes a transition metal such as molybdenum (Mo), tungsten (W), niobium (Nb), rhenium (Re), or Titanium (Ti), and X is a chalcogen such as sulfur (S), selenium (Se), or tellurium (Te). TMDC materials have been studied largely by experiments and ab-initio calculations. The TMDC semiconductors have the energy band-gap ranging from below $1\ eV$ to above $2.5\ eV$ [31, 32]. This behavior opens new opportunities for constructing devices that feature light generation functions, such as light-emitting diodes (LEDs). Additionally, the valley coherence and valley-selective circular dichroism, observed in various monolayer TMDCs, offer novel physical phenomena that can be explored for novel applications in optical computing and communications.

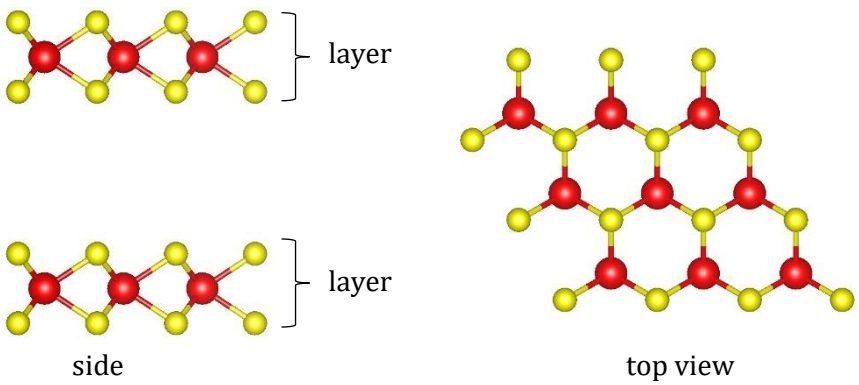

Figure 4.1 Lattice structure of MoS_2 layer (side view and top view), where red atoms represent Mo and yellow atoms represent S. A typical isotropic sandwich structure and honeycomb structure of TMDC. And inter-layer interaction is mediated by the weak van der Waals force.

Molybdenum disulfide (MoS_2) is a prototypical TMDC, which is composed of 2D S, Mo, S sheets stacking on top of one another, as shown in Figure 4.1. The inter-layer interaction of MoS_2 is mediated by the weak van der Waals force, while the in-plane bonding is the strong covalent bond. Thus, bulk MoS_2 can be exfoliated down to a single or few-layer nanosheets like graphene. Also, it has an indirect bandgap in its multi-layer forms, however it becomes a direct-bandgap semiconductor in its monolayer form. The direct bandgap of the MoS_2 monolayer leads to efficient light emission. This is similar to tungsten-based dichalcogenides (for example WS_2) [9, 33], making them suitable for developing optoelectronic devices. Recently, there have been a few studies on alloying between MoS_2 and WS_2. They found that, the resultant bandgap can be continuously tuned [34].

In this thesis, we performed the first-principle study on a TMDC monolayer of MoS_2 and WS_2 to calculate the bonding distance, cell parameter and band structure. Then we modelled the alloying $Mo_{1-x}W_xS_2$ monolayer supercells by using the Special Quasirandom Structures (SQS) method. The development of the band gap and band alignment of $Mo_{(1-x)}W_xS_2$ for each variation as a function of the W concentration will be extensively investigated.

Table 1 The primitive cell structure of hexagonal MoS_2 monolayer							
The lattice parameter of MoS_2 monolayer (vector)				The atomic positions of MoS_2 monolayer			
					a	b	c
a	3.1500	0.0000	0.0000	Mo	0.333333	0.666667	0.125000
b	-1.5750	2.7279	0.0000	S	0.666667	0.333333	0.189255
c	0.0000	0.0000	24.5900	S	0.666667	0.333333	0.060750

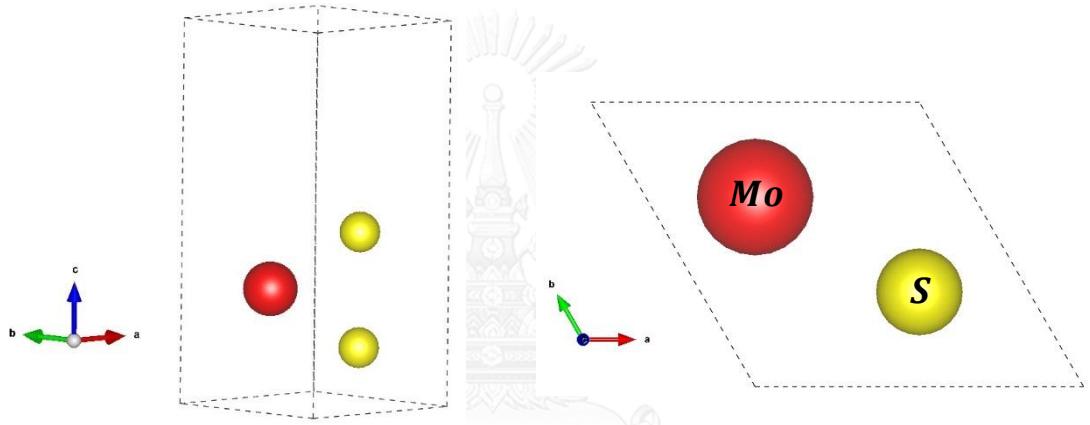

Figure 4.2 Side view (left) and Top view (right) of the primitive cell structure of hexagonal MoS_2 monolayer with line of unit cell.

4.1.1 Calculation parameters for the first-principle calculation

The hexagonal structure of MoS_2 monolayer with a lattice parameter and atomic positions as Table 1, that was taken as the starting point for the first-principle calculations. The first-principle calculations were performed within the density functional theory (DFT) as mention in Chapter 2. The exchange correlation functional using the generalized gradient approximation (GGA), as implemented in the Quantum ESPRESSO package (see Appendix A). The atomic cores of the TMDC were represented by using ultrasoft pseudopotentials [24]. The electronic wavefunctions were described by the plane-wave basis sets. So, when we make a DFT calculation with plane-waves basis sets, the electronic wavefunction is represented by the infinite summation of plane waves, which must be truncated, to be able to handle them

computationally. So, the more plane waves, the more accuracy, but also higher computational cost.

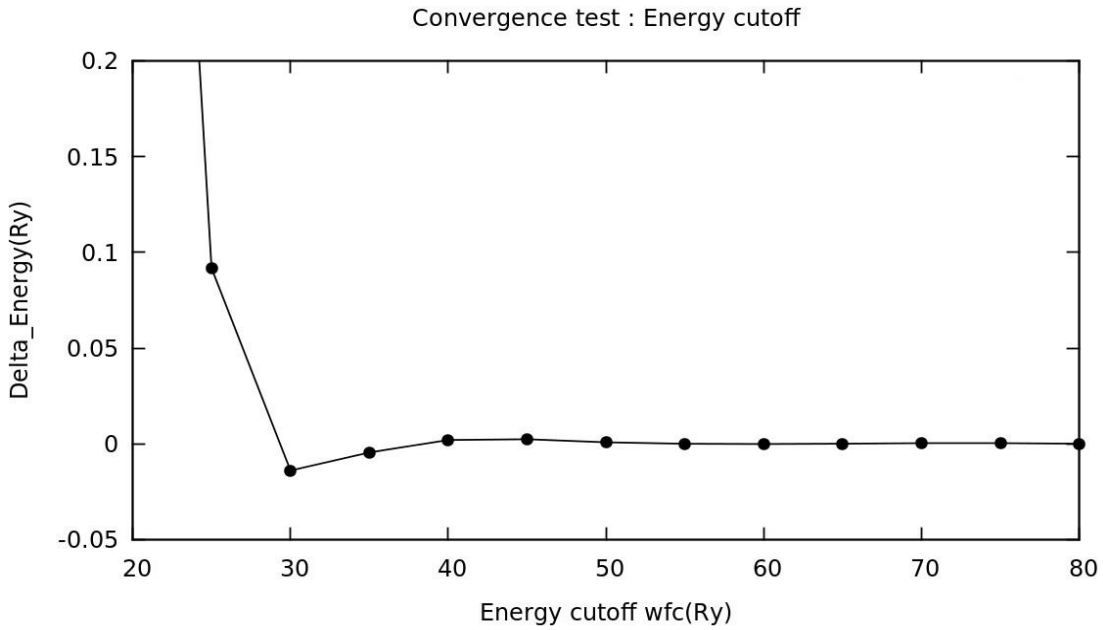

Figure 4.3 Graphs of the convergence test by optimum energy cutoff wfc from 20 to 80 Ry. As shown in the figure, the best choice for the energy cutoff wfc value seems to be 60 Ry (because energy difference between 60 to 80 Ry is close to zero) for this pseudo potential.

The technique for speeding up the calculations relies on the fact that the plane waves with less kinetic energy have higher contribution to the totality, so the plane waves with lower energy are the most important. But, up to which point should we increase the cutoff, so that we get a good balance between computational cost and accuracy. That is precisely the optimum cutoff choice. The convergence test by optimum energy cutoff wavefunction show in Figure 4.3

The next parameter for setup DFT calculation on Quantum ESSPRESSO package is kinetic energy cutoff (ecutrho) for charge density and potential with ultrasoft pseudopotentials. By default, ecutrho is set to 4 times of energy cutoff, but in this studied system the exchange correlation functional using GGA functional, especially in

cells with vacuum usually requires higher values of ecutrho to be accurately converged. So, the convergence test by optimum ecutrho show in Figure 4.4

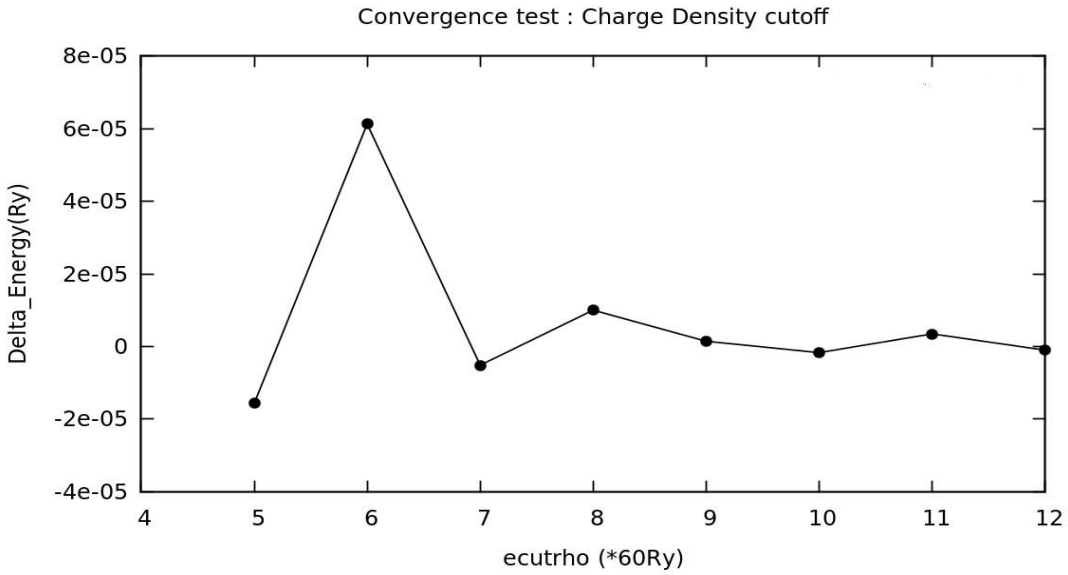

Figure 4.3 Graphs of the convergence test by optimum ecutrho from 300 to 720 Ry. As shown in the figure, the energy difference converges at 540 Ry. The best choice for the ecutrho value should be 540 Ry for this system.

And one should look for convergence at small values of the broadening. For a periodic system, integrals in real space over the infinitely extended system are replaced by integrals over the finite first Brillouin zone in reciprocal space, by virtue of Bloch's theorem in Chapter 2. The integrals are performed by summing the function values of the integrand the charge density at a finite number of points in the Brillouin zone, called the k-point mesh. Choosing a sufficiently dense mesh of integration points is crucial for the convergence of the results, and is therefore one of the major objectives when performing convergence tests. Here it should be noted that there is no variationally principle governing the convergence with respect to the k-point mesh. This means that the total energy does not necessarily show a monotonous behavior when the density of the k-point mesh is increased. Here a rather arbitrary but standard choice of uniform Monkhorst-Pack mesh grids. By choosing automatic k-point mesh, the calculation automatically generated uniform grid of k-points. The first Brillouin

zone is sampled with a nk × nk × 1 Monkhorst-Pack grid for the monolayer system. So, the convergence test by k-point show in Figure 4.5

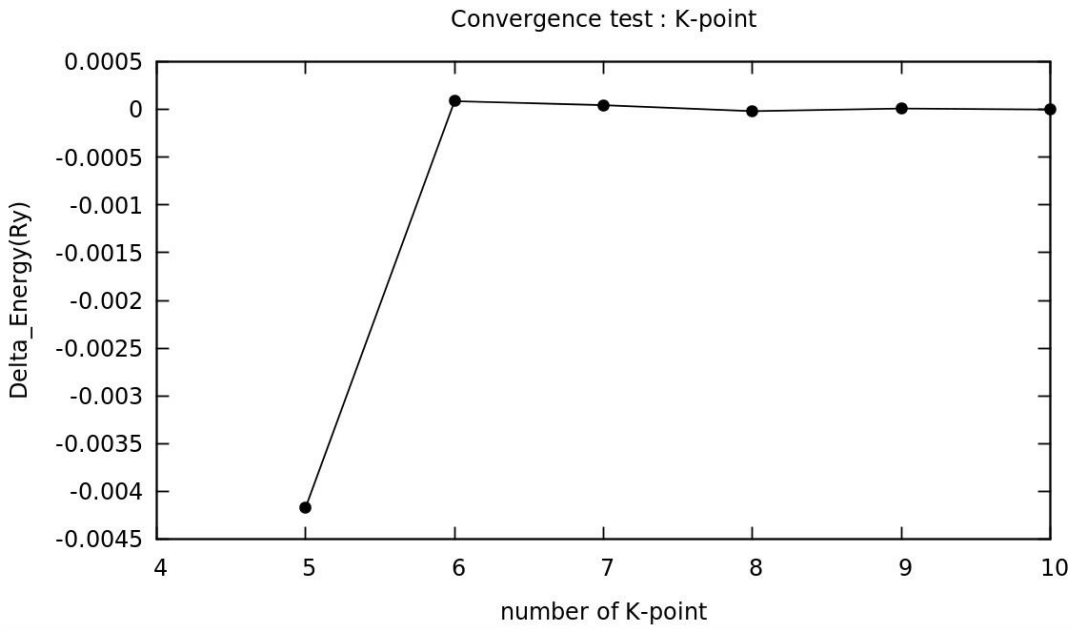

Figure 4.5 Graphs of the convergence test by number of k-point from nk = 5 to 10. As shown in the figure, the energy difference converges at nk = 8. The choice for the nk value be 8 for this system. So, the first Brillouin zone is sampled with a 8 x 8 x1 Monkhorst-Pack grid.

Now, we have the necessary calculation parameters for the first principle calculation on Quantum ESPREESO package likes a physical structure and a band structure. In addition, the Tungsten disulfide WS_2 also use the same calculation parameters due to the similar structure of the material. By the way, the next section will show the result of the calculation, which will show that MoS_2 and WS_2 can alloying together.

4.1.2 Structural relaxation and band structure calculation

The hexagonal structure of MoS_2 and WS_2 with the lattice parameters from previous section was taken as the starting point for the geometry relaxation. The optimization of initial structures was performed using analytical energy gradients with respect to atomic coordinates and unit cell parameters within a quasi-Newton scheme combined with the BFGS (Broyden-Fletcher-Goldfarb-Shanno) scheme for Hessian. The

optimized lattice parameters are given in previous section (Table 1). By calculating the total forces acting on each atom until the total forces overall the cell are less than 10^{-6}eV/Å. And with variable-cell optimization (vc-relax), that vc-relax are performed with plane waves and G-vectors calculated for the starting cell. Because we aiming to study monolayer (2D), thus for convenience the band structures were calculated along the high symmetry points following the $\text{K}-\Gamma-\text{M}-\text{K}$ path as shown in Figure 4.6. The results of the lattice parameters, bond angle and energy gap are shown in Table2.

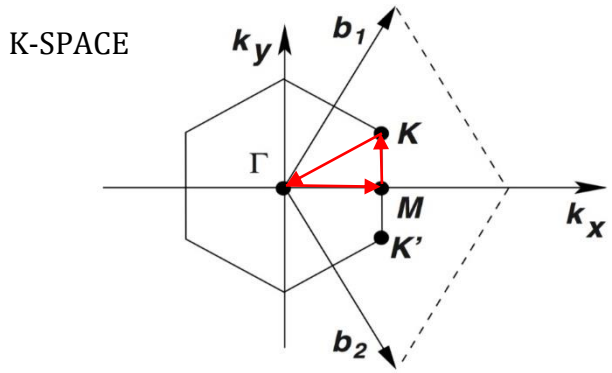

Figure 4.6 First Brillouin zone of hexagonal structure and its high symmetry points. The following path for band calculation as shown by red arrows.

Table 2 Calculated structural parameters (atom distances d_{Mo-S}, d_{W-S}; separation of the metal and sulfur layers d_{thick}; bond angle, θ_{S-Mo-S}, θ_{S-W-S}) and energy band gap, E_g of the MoS_2 and WS_2 monolayers. Comparable with the other work (in bracket) and experiment result [35, 36, 37,38]

	Calculation					Experiment	
MoS_2	$a(\text{Å})$	$d_{Mo-S}(\text{Å})$	$d_{thick}(\text{Å})$	θ_{S-Mo-S}	$E_g(eV)$	$a(\text{Å})$	$E_g(eV)$
	3.19(3.19)	2.42(2.43)	1.56(1.56)	80.67(80.68)	1.80(1.72)	3.17	1.90
WS_2	$a(\text{Å})$	$d_{W-S}(\text{Å})$	$d_{thick}(\text{Å})$	θ_{S-W-S}	$E_g(eV)$	$a(\text{Å})$	$E_g(eV)$
	3.19(3.19)	2.42	1.56(1.56)	80.95	2.00(2.10)	3.162	2.07

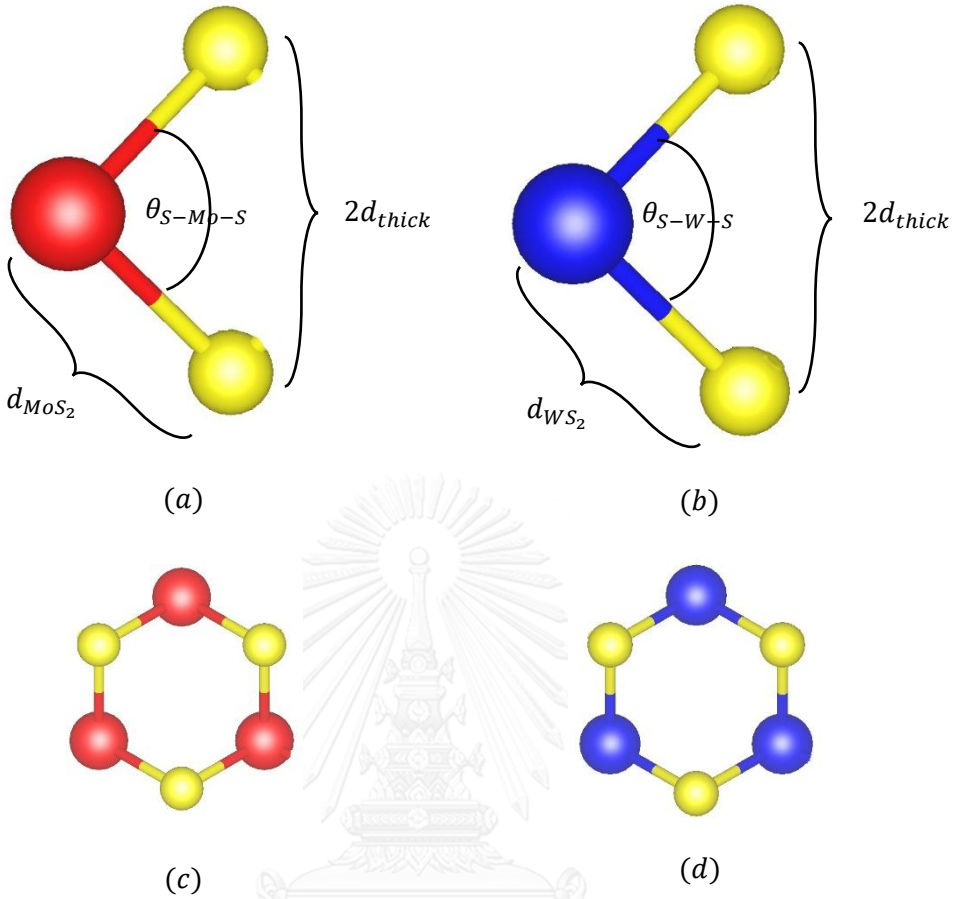

(a) (b)

(c) (d)

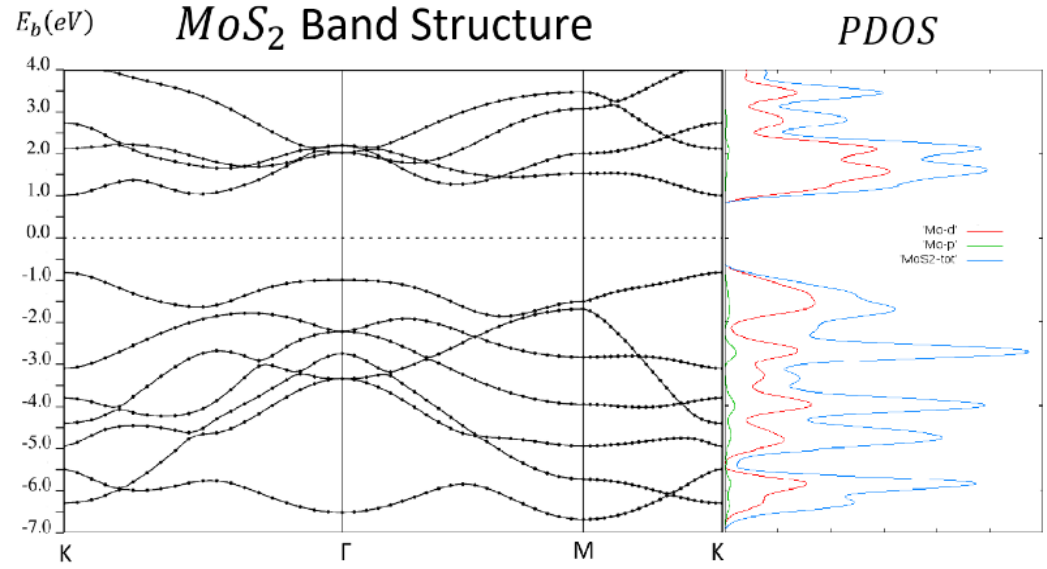

(e)

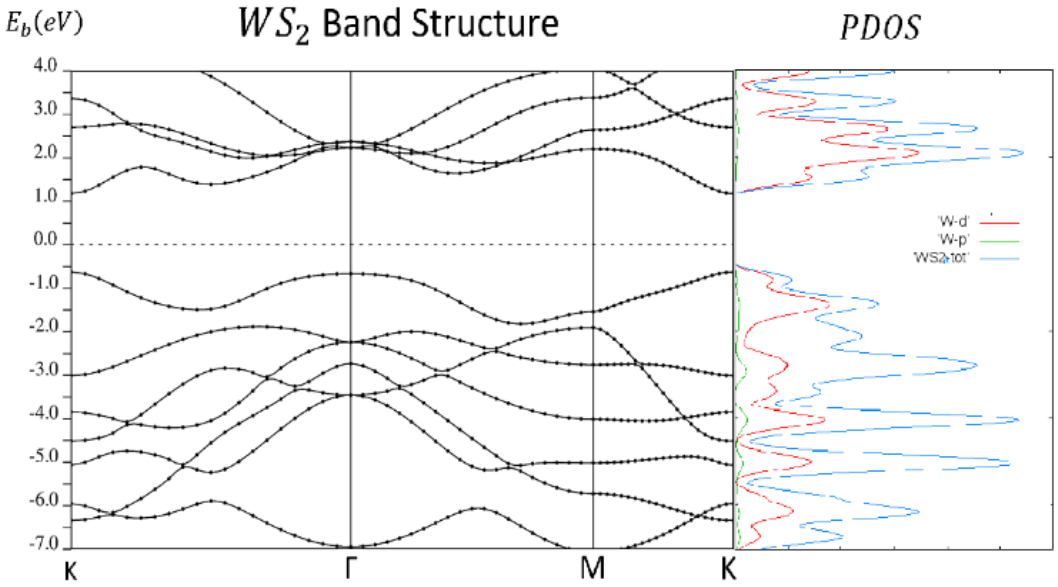

(f)

Figure 4.7 $(a), (b)$ characteristic of MoS_2 and WS_2 respectively $(c), (d)$ hexagonal structure of MoS_2 and WS_2 (e) band structure and project density of state (PDOS) of MoS_2 (f) band structure and PDOS of WS_2, There are direct band gap at K-point both MoS_2 and WS_2

We have obtained a remarkable result. The computed energy band gaps (E_g) of the MoS_2 and WS_2 monolayers (1.80 eV and 2.00 eV) are in good agreement with experimental results [35,36].

4.2 Modeling of $Mo_{1-x}W_xS_2$ using Special Quasirandom Structure method

Our model structure of $Mo_{1-x}W_xS_2$ is generated by the SQS, using the pair correlation functions with spanning distance up to the ninth atomic neighbor shells. First, we investigate suitable size of supercell by comparable the pair correlation functions and total correlation error between various sizes of supercells (2x2x1, 3x3x1 and 4x4x1). In Table 3, There are obviously noticeable that 2x2x1 supercell is preferred order atomic arrangement. And we found 3x3x1 supercell is suitable size of supercell, because the total correlation error values are not much difference than 4x4x1 supercell. So, we chose a 3x3x1 supercell with 27 atoms per supercell. By comparison of the ensemble average of the pair correlation functions $\langle\overline{\Pi}_{2,m}(S)\rangle$ for each arrangement of atoms in the model structure with $\langle\overline{\Pi}_{2,m}\rangle_R$, we can choose any structure that gives the best match. Some $\langle\overline{\Pi}_{2,m}(S)\rangle$ of chosen configurations are shown in Table 4. The crystal structures of $Mo_{1-x}W_xS_2$ at $x = 0.11$ of the 3x3x1 supercell have all possible $\frac{9!}{1!8!} = 9$ configurations. The SQS shows that every configuration has the same value for pair correlation functions up to the ninth atomic neighbor shells, so we choose one of them, and denoted by SQS-1. In the same way, as $x = 0.22$, the supercell has all possible $\frac{9!}{2!7!} = 36$ configurations and the SQS can be distributed into 2 groups by the value of correlation functions, denoted by SQS-2 and SQS-3. For $x = 0.33, 0.44$ the SQS can be distributed into 3 groups. The result shows that most of the pair correlation functions are closed to random except for the pair correlation function of fifth atomic neighbor shell. Note that the fifth atomic neighbor shell is far from perfect random configuration, which probably happens because we use small periodic supercell. However, the total correlation error is comparable with the random correlation. For the 3x3x1 supercell, our chosen structures produce the value of pair correlation function $\langle\overline{\Pi}_{2,m}\rangle(S)$ closed to the perfect random configuration $\langle\overline{\Pi}_{2,m}\rangle_R$. Thus, the 3x3x1 supercell is reasonable for the small periodic unit cell that

can represent the perfect random alloy, and can be used to study the formation energy and band gaps in the next section.

Table 3 The pair correlation functions and the total correlation error ($Error_{2,m} = \frac{\sum_{m=1}^{9}(|\langle\overline{\Pi}_{2,m}\rangle(S)-\langle\overline{\Pi}_{2,m}\rangle_{Random}|)}{9}$) comparison between various sizes of supercells by similar of W concentration.

	2x2x1 supercell				3x3x1 supercell				4x4x1 supercell			
x%	25%		50%		22%		44%		25%		43.75%	
Figure	random		random		random		random		random		random	
$\langle\overline{\Pi}_{2,1}\rangle$	0.250	0.000	0.000	-0.333	0.309	0.259	0.012	-0.037	0.250	0.167	0.016	-0.083
$\langle\overline{\Pi}_{2,2}\rangle$	0.250	0.000	0.000	-0.333	0.309	0.111	0.012	0.333	0.250	0.250	0.016	0.000
$\langle\overline{\Pi}_{2,3}\rangle$	0.250	1.000	0.000	1.000	0.309	0.259	0.012	-0.037	0.250	0.167	0.016	-0.083
$\langle\overline{\Pi}_{2,4}\rangle$	0.250	0.000	0.000	-0.333	0.309	0.259	0.012	0.037	0.250	0.250	0.016	0.000
$\langle\overline{\Pi}_{2,5}\rangle$	0.250	0.000	0.000	-0.333	0.309	1.000	0.012	1.000	0.250	0.167	0.016	-0.083
$\langle\overline{\Pi}_{2,6}\rangle$	0.250	1.000	0.000	1.000	0.309	0.111	0.012	-0.333	0.250	0.167	0.016	-0.083
$\langle\overline{\Pi}_{2,7}\rangle$	0.250	0.000	0.000	-0.333	0.309	0.259	0.012	-0.037	0.250	0.167	0.016	-0.083
$\langle\overline{\Pi}_{2,8}\rangle$	0.250	1.000	0.000	1.000	0.309	0.259	0.012	-0.037	0.250	1.000	0.016	1.000
$\langle\overline{\Pi}_{2,9}\rangle$	0.250	0.000	0.000	-0.333	0.309	0.259	0.012	-0.037	0.250	0.083	0.016	0.000
$Error_{2,m}$	0.000	0.417	0.000	0.555	0.000	0.154	0.000	0.219	0.000	0.148	0.000	0.169

Table 4 The pair correlation functions and the total correlation error ($Error_{2,m} = \frac{\sum_{m=1}^{9}(|\langle\overline{\Pi}_{2,m}\rangle(S)-\langle\overline{\Pi}_{2,m}\rangle_{Random}|)}{9}$) of the optimum SQS with 27-atom supercell for each W concentration.

Figure	x=0.11		x=0.22			x=0.33				x=0.44			
	random	SQS-1	random	SQS-2	SQS-3	random	SQS-4	SQS-5	SQS-6	random	SQS-7	SQS-8	SQS-9
$\langle\overline{\Pi}_{2,1}\rangle$	0.605	0.556	0.309	0.259	0.111	0.111	0.111	-0.037	-0.333	0.012	-0.037	-0.185	-0.333
$\langle\overline{\Pi}_{2,2}\rangle$	0.605	0.556	0.309	0.111	0.556	0.111	-0.333	0.111	1.000	0.012	-0.333	0.111	0.556
$\langle\overline{\Pi}_{2,3}\rangle$	0.605	0.556	0.309	0.259	0.111	0.111	0.111	-0.037	-0.333	0.012	-0.037	-0.185	-0.333
$\langle\overline{\Pi}_{2,4}\rangle$	0.605	0.556	0.309	0.259	0.111	0.111	0.111	-0.037	-0.333	0.012	-0.037	-0.185	-0.333
$\langle\overline{\Pi}_{2,5}\rangle$	0.605	1.000	0.309	1.000	1.000	0.111	1.000	1.000	1.000	0.012	1.000	1.000	1.000
$\langle\overline{\Pi}_{2,6}\rangle$	0.605	0.556	0.309	0.111	0.556	0.111	-0.333	0.111	1.000	0.012	-0.333	0.111	0.556
$\langle\overline{\Pi}_{2,7}\rangle$	0.605	0.556	0.309	0.259	0.111	0.111	0.111	-0.037	-0.333	0.012	-0.037	-0.185	-0.333
$\langle\overline{\Pi}_{2,8}\rangle$	0.605	0.556	0.309	0.259	0.111	0.111	0.111	-0.037	-0.333	0.012	-0.037	-0.185	-0.333
$\langle\overline{\Pi}_{2,9}\rangle$	0.605	0.556	0.309	0.259	0.111	0.111	0.111	-0.037	-0.333	0.012	-0.037	-0.185	-0.333
$Error_{2,m}$	0.000	0.087	0.000	0.154	0.264	0.000	0.198	0.198	0.592	0.000	0.219	0.263	0.461

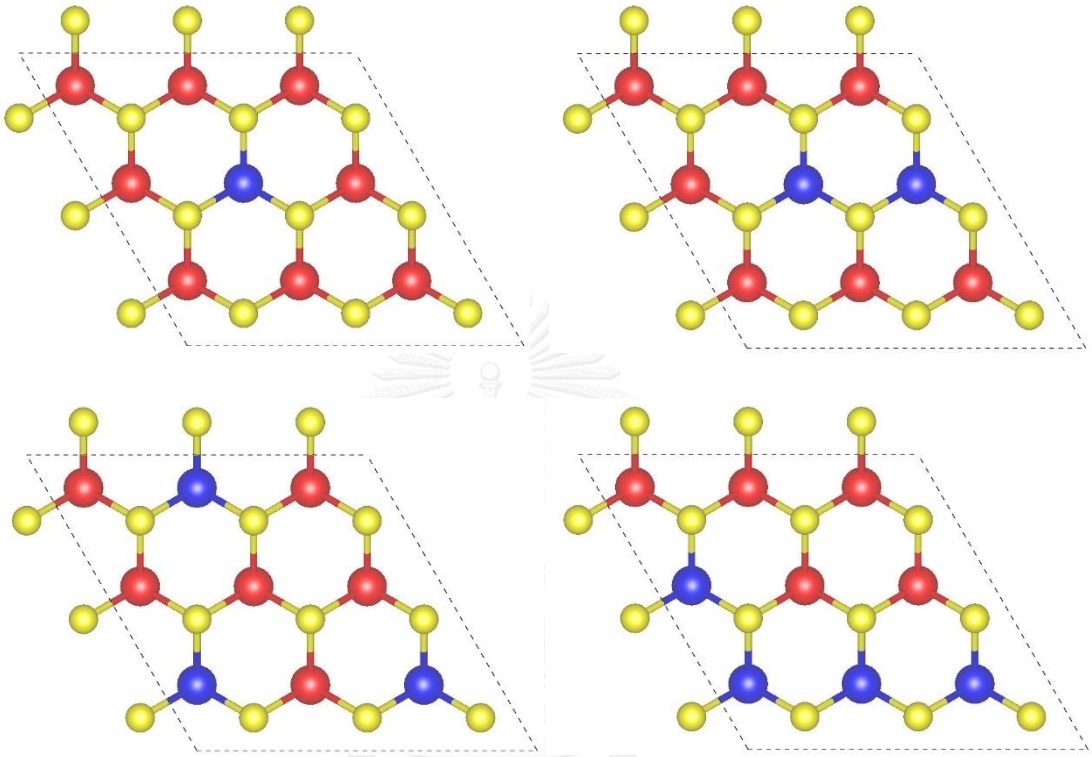

Figure 4.8 Top view on the structure of the configuration SQS of 3x3x1 supercell $Mo_{1-x}W_xS_2$ at $x = 0.11, 0.22, 0.33, 0.44$, where Mo are red atoms, $W$are blue atoms and S are yellow atoms.

For x = 0.56, 0.67, 0.78 and 0.89, we have used the same arrangement of atoms but swap the positions of Mo and W atom. So that, the SQS reduce all possible configurations for 3x3x1 supercell (510 configurations) to the 9 SQS groups of atomic arrangements in the model structure. This reduces the number of the model structure to be used in the density functional theory calculations. There is no need to examine all possible configurations of the atomic arrangements.

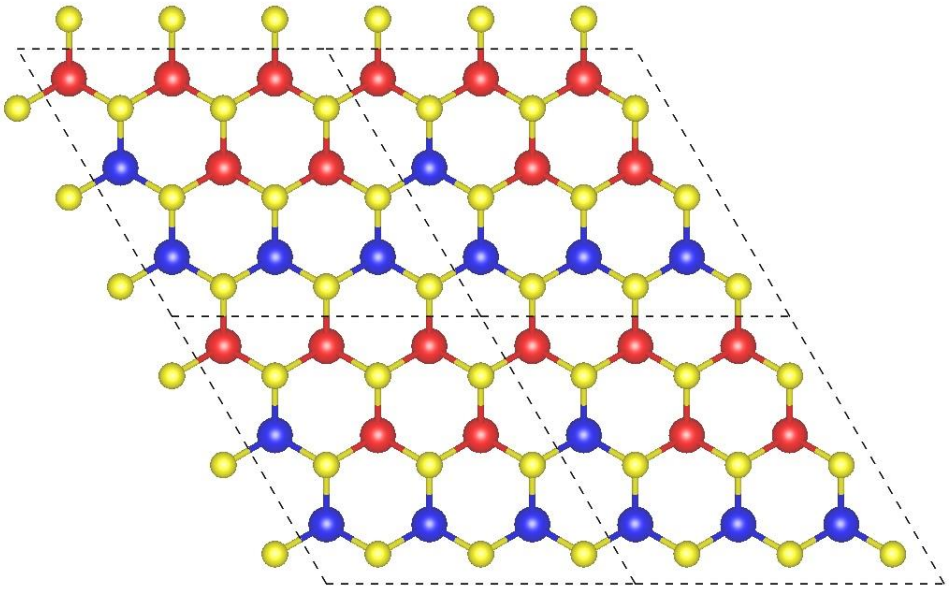

Figure 4.9 An alternative point of view of the periodic supercell $Mo_{1-x}W_xS_2$ at $x = 0.44$ From the Table 4 that the fifth atomic neighbor shell is far from perfect random configuration, which probably happens because we use small periodic supercell.

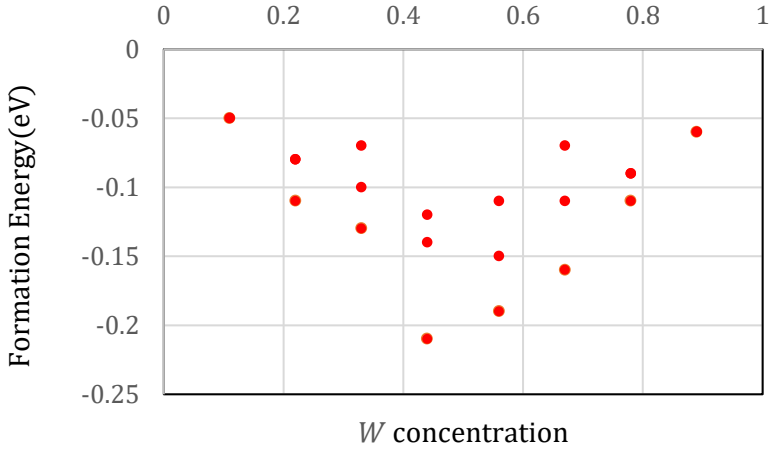

Figure 4.10 Chart of the formation energy as a function of W concentration. Each point is the formation energy of the model structure $Mo_{1-x}W_xS_2$ that was generated by SQS method from Table 4.

The total energy (E_{tot}) for each arrangement of $Mo_{1-x}W_xS_2$ alloy is calculated as well as the alloy formation energy for each W concentration, $E_f(x) = E_{tot} - (1-x)E_{MoS_2} -$

xE_{WS_2} where x is the concentration of W, E_{MoS_2} and E_{WS_2} are the total energies per formula unit of MoS_2 and WS_2 calculated from the previous section. The formation energy as a function of W concentration is shown in Figure 4.10. The negative values suggest that the miscible alloys can be formed. Then, we take the structure with the lowest formation energy to examine the band structure in the next chapter.

CHAPTER 5

ELECTRONICAL PROPERTY OF ALLOY $Mo_{1-x}W_xS_2$ MATERIALS BY USING SPECIAL QUASIRANDOM STRUCTURE

Results and Discussion

The electronic band structure of the supercell is quite complex. Hence the unfolding of the bands needs to be performed (see Appendix B) [39, 40]. Then we investigate the results of the band gaps and band edges of the $Mo_{1-x}W_xS_2$ alloys. The results show that the band gap moderately decreases from x= 0 to 0.33 and moderately increases from x=0.33 to 0.67 and then the band gap is rising more rapidly from x=0.67 to 1 (see Figure 5.1). The results resemble a parabolic characteristic or a bowing effect of the band gap. The modification of the band gap by variating the W concentration can expand into the application of nanoelectronics and optoelectronics.

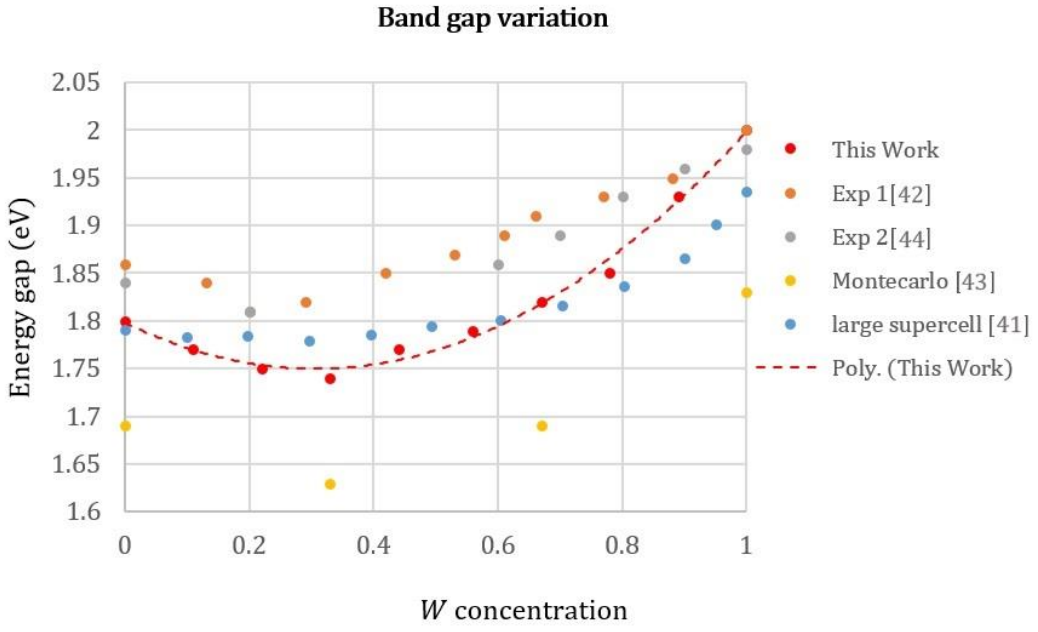

Figure 5.1 Band gap variation shows that the electronic property, energy band E_g, which are calculated from the special supercell generated by SQS method give comparable results with other method and experiment.

For the band edges of the conduction band and the valence band from x=0 to 0.44, the conduction band minimum (below Fermi level) shifts only a little whereas the valence band (above Fermi level) shifts significantly. In contrast, from x=0.56 to 1, the results show that the conduction band shifts more significantly than that of the valence band (see Figure 5.2). From the results of the band edges, it can be concluded that if the W concentration is dominating the Mo concentration in the $Mo_{1-x}W_xS_2$ alloys, then the conduction band is swung by WS_2, and vice versa if MoS_2 dominates then the valence band is swung. Since the valence band maxima of MoS_2 and WS_2 originate from the d_{xy} and $d_{x^2-y^2}$ orbitals of the metal, doping a W atom in MoS_2 instantly shifts them up in energy. In contrast, the conduction band minimum is dominated by the d_{z^2} of the metal in the case of MoS_2 but the d_{xy}, $d_{x^2-y^2}$, and d_{z^2} states in the case of WS_2 , which is described by density of states for the valence and conduction bands in these works [41, 42]. For x=0 to 0.33 W contributes slightly to the conduction band minimum, resulting in small energetic upshifts. For x=0.33 to 1, the W contribution becomes dominant and thus the upshifts are enhanced. This feature can be described by the different positions of the band edges in MoS_2 and WS_2.

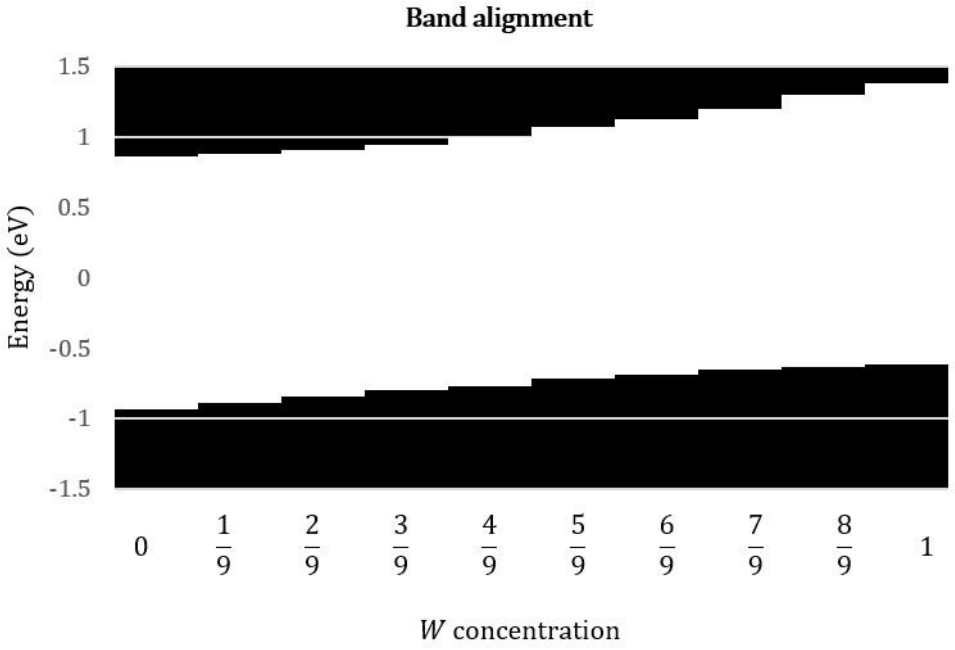

Figure 5.1 The band alignment (eV) of the $Mo_{1-x}W_xS_2$, the Fermi level is set to 0 eV for all the W concentration varies by $x = 0, \frac{1}{9}, \frac{2}{9}, \ldots, 1$.

In conclusion, the atomic distributions in the monolayer semiconducting transition metal dichalcogenide $Mo_{1-x}W_xS_2$ alloys have been investigated by using the density functional theory and modeling by the special quasi-random structure customized for the 2D material. We showed that this model can describe the nature of the 2D band structure and is in good agreement with the result from the first-principle calculation by Monte Carlo simulations [43], a large supercell calculation [41], and experimental results [42, 44]. This is remarkable that using small periodic cell (3x3x1 with 27 atoms in the model structure) generated by the SQS can be used very well. Although this model only exists at low temperature according to the SQS and the DFT simulation. The Negative formation energies suggest a good miscibility for the $Mo_{1-x}W_xS_2$ alloys. Our results demonstrate that the band gaps and band edges can be varied continuously in the $Mo_{1-x}W_xS_2$ monolayer alloys, with the minimum gap appearing at around x = 0.33. The tunable band gap by alloying could strongly broaden the range of possible applications of the transition metal dichalcogenide monolayers.

As mentioned above the 2D SQS $Mo_{1-x}W_xS_2$ is one of the interesting ways that using for studies another physical and electronical properties. With using small periodic cell that suitable for DFT calculations that explain the goods meaning of physics than another method likes Monte Carlo simulations. In addition, by decreasing the number of atoms in supercell (likes large supercell approach), cause decrease the computational cost and calculation time. This SQS method increase performance for any condensed matter studied that using computation explicitly.

From the above results, the Special Quasirandom Structure (SQS) method works well for 2D material (Transition metal dichalcogenides in this thesis), especially with the band structure. In the Chapter 6, we will summarize the results and discuss about limitation of the SQS method.

CHAPTER 6

CONCLUSION

This thesis has shown that it is possible to model special periodic supercells structure with binary atoms arrangement ($A_{1-x}B_x$) such that the correlation functions closely reproduce those in a perfectly random infinite pseudo-binary alloy. Physical and electronical properties that depend on the local atomic structure of the alloy can be described by using DFT calculation on the Special Quasirandom Structure. The characteristic of SQS has those features: (1) short-periodic supercell in unusual orientations, with (2) just a few atoms per cell, and with (3) site symmetries that are distinctly lower than another order structure likes constituent solids (charcoal pyrite or copper-gold structure). For the electronical property that represent by the SQS is within the local density formalism reveals significant atomic relaxations consistent with the lower symmetry of atoms in the alloy (using periodic supercell on DFT). This leads to (1) substantial lowering of the alloy's formation enthalpies, (2) the band structure of the sample structure and (3) optical bowing of the band gaps (TMDC alloy materials in this work). Those structure are generated by the SQS method can be readily generalized to other compositions, symmetries, and to imperfectly disordered alloys and affords accurate descriptions of physical and electronical properties of alloys within any DFT based calculation.

In addition, the SQS method is possible to design special structures with small number of atom. This mean that computational cost and time are rapidly decrease for DFT calculation. Both results imply that we are possible to manage or design other problems (experiment and simulation) that are more difficult than ever. For example, the model of many-layers with trapping molecule or atoms need a lot of computational cost to simulate its besides if that model increases other complexity likes disorder effect, then computational cost goes up. So, the SQS with small number

of atom can match up this problem by decrease number of atom on model that are used for calculation.

By the way, the SQS has some limitation, this method is not available in all cases especially the model structure with higher symmetry of atoms. Other than that, it cannot be used for complex alloy (like interstitial alloy or more than binary compound). But if the system studied is binary or pseudo-binary substitution alloy, the SQS method work wells for generate the special structure which is used by DFT calculation.

REFERENCES

[1] Landau, Rubin H. Paez, Jose Bordeianu and C. Cristian A survey of computational physics: introductory computational science. (2011)

[2] H. M. Ledbetter. “Estimation of Debye temperatures by averaging elastic coefficents”. J. Appl. Phys. (1973) 44, 1451

[3] H. M. Ledbetter. Handbook of Elastic Properties of Solids, Liquids, Gases, Volume III, Levy, Bass, and Stern (ed.) (2001)

[4] Althoff, J. D. etal. “Vibrational spectra in ordered and disordered Ni_3Al”. Phys. Rev. B (1997) 56, R5705

[5] Ravelo, T., et al. ‘’Free energy and vibrational entropy difference between ordered and disordered Ni_3Al”. Phys. Rev. B (1998) 57, 862

[6] “Physics History: October 22, 2004: Discovery of Graphene”. APS News. Series II. 18(9): 2. 2009

[7] Freitag, M. “Graphene: Nanoelectronics goes flat out”. Nat. Nanotechnol. (2008) 3, 455-457

[8] De Abajo, F. J. G. “Graphene nanophotonics”. Science (2013), 339, 917-918.

[9] A. Kuc, N. Zibouche, and T. Heine. “Influence of quantum confinement on the electronic structure of the transition metal sulfide”. Phys. Rev. B (2011) 24

[10] M. Born and T. Oppenheimer. “Zur Quantentheorie der Molekeln”. Annalen der Physik (1927) 389, 714-733.

[11] F. Bloch. “Uber die quantenmechanic der elektronen in kristallgittern”. Zeitschrift fur Physik (1928) 52, 555.

[12] P. Hohenberg and W. Kohn. “Inhomogeneous electron gas”. Phys. Rev. B (1964) 136, 864-871.

[13] W. Kohn and L. J. Sham. “self-consistent equations including exchange and correlation effects” Phys. Rev. A 140.4A (1965), 1133-1138.

[14] D. M. Ceperley and B. J. Alder. “Ground state of the electron gas by a stochastic method”. Physical Review Letters (1980) 45, 566-569.

[15] R. M. Martin. “Electronic structure, basic theory and pratical methods”. Cambridge university Press (2004)

[16] O. Gunnarsson, M. Jonson, and B. I. lundqvist. “Descriptions of exchange and correlation effects in inhomogeneous electron systems”. Phys. Rev. B (1979) 20, 3136.

[17] A. D. Becke. “Density functional exchange-energy approximation with correct asymptotic behavior”. Phys. Rev. A (1988) 38, 3098.

[18] Y. Wang and J. P. Perdew. “Correlation hole of the spin-polarized electron gas, with exact small-wave-vector and highdensity scaling”. Phys. Rev. B (1991) 44, 13298.

[19] J. Perdew, K. Burke, and M. Ernzerhof. “Generalized Gradient Approximation Made Simple”. Physical Review Letters (1996) 77, 3865.

[20] P. Giannozzi, S. Baroni, N. Bonini, M. Calandra, R. Car, C. Cavazzoni, D. Ceresoli, G. L. Chiarotti, M. Cococcioni, I. Dabo, A. Dal Corso, S. Fabris, G. Fratesi, S. de Gironcoli, R. Gebauer, U. Gerstmann, C. Gougoussis, A. Kokalj, M. Lazzeri, L. Martin-Samos, N. Marzari, F. Mauri, R. Mazzarello, S. Paolini, A. Pasquarello, L. Paulatto, C. Sbraccia, S. Scandolo, G. Sclauzero, A. P. Seitsonen, A. Smogunov, P. Umari, R. M. Wentzcovitch, J. Phys. Condens Matter (2009) 21, 395502.

[21] H. Hellmann. “A new approximation method in the problem of many electrons”. The Journal of Chemical Physics (1935), 61.

[22] H. Hellmann and W. Kassatotschkin. “Metallic binding according to the combined approximation procedure”. The Journal of Chemical Physics (1936), 324.

[23] D. R. Hamann, M. Schluter, and C. Chiang. “Norm-Conserving Pseudopotentials”. Physical Review Letters (1979) 43, 1494.

[24] D. Vanderbilt. “Soft self-consistent pseudopotentials in a generalized eigenvalue formalism”. Phys Rev. B (1990) 41, 7892.

[25] K. Binder, J.L. Lebowitz, M. K. Phani, and M. H. Kalos, Acta. Metall. ”Application of Monte Carlo Method in-Statistical Physics, 2nd ed., edited by K. Binder” Springer-Verlag, Berlin (1989).

[26] S. Lee, D. M. Bylander, and L. Kleinman, Phys. Rev. B (1989) 40, 8399.

[27] J. M. Sanchez, F. Ducastelle, and D. Gratias. “Generalized cluster description of multicomponent systems”. Physica A: Statistical Mechanics and its Applications (1984) 1128, 334-350.

[28] A. V. Ruban and I. A. Abrikosov. “configurational thermodynamics of alloys from fitst principles: effective cluster interactions”. Reports on Progress in Physics (2008) 71, 046501.

[29] S-H. Wei, A. Mbaye, L. G. Ferreira, and A. Zunger, Phys. Rev. B (1987) 36, 4163; A. Zunger, S.-H. Wei, A. Mbaye, and L. G. Ferreira, Acta. Metall. (1988) 36, 2239.

[30] A. Zunger et al. “Special Quasirandom Structures”. Physical Review Letters (1990) 65.3, 353.

[31] Wang, Q. H., Kalantar-Zadeh, K., Kis, A. and Coleman, J. N.; Strano, M. S. “Electronics and optoelectronics of two- dimensional transition metal dichalcogenides”. Nat. Nanotechnol. (2012) 7, 699–712.

[32] Peng B., Ang, P. K. and Loh K. P., “Two-dimensional dichalcogenides for light-harvesting applications”. Nano Today (2015) 10, 128–137.

[33] Zhao H., Guo Q. S., Xia F. N. and Wang H., “Two-dimensional materials for nanophotonics application”. Nanophotonics (2015) 4.

[34] Chen, Y. F.; Dumcenco, D. O.; Zhu, Y. M.; Zhang, X.; Mao, N. N.; Feng, Q. L.; Zhang, M.; Zhang, J.; Tan, P.-H.; Huang, Y.-S. et al. “Composition-dependent Raman modes of $Mo_{1-x}W_xS_2$ monolayer alloys”. Nanoscale (2014) 6, 2833–2839.

[35] Lee, H. S.; Min, S.-W.; Chang, Y.-G.; Park, M. K.; Nam, T.; Kim, H.; Kim, J. H.; Ryu, S.; Im, S. “MoS2 nanosheet phototransistors with thickness-modulated optical energy gap”. Nano Lett. (2012) 12, 3695–3700.

[36] Jo, S.; Ubrig, N.; Berger, H.; Kuzmenko, A. B.; Morpurgo, A. F. “Mono- and bilayer WS2 light-emitting transistors”. Nano Lett. (2014), 14, 2019–2025.

[37]Zhu ZY, Cheng YC, Schwingenschlögl U “Giant spin-orbit-induced spin splitting in two-dimensional transition-metal dichalcogenide semiconductors”. Phys Rev B (2011) 84.

[38] Ataca, C.; S-ahin, H.; Akturk, E.; Ciraci, S. “Mechanical and Electronic Properties of MoS2 Nanoribbons and Their Defect”. J. Phys. Chem. C 2011, 115, 3934–3941.

[39] Paulo V. C. Medeiros, Sven Stafström and Jonas Björk, Phys. Rev. B 89, 041407(R) (2014)

[40] Paulo V. C. Medeiros, Stepan S. Tsirkin, Sven Stafström and Jonas Björk, Phys. Rev. B. (2015) 91, 041116.

[41] Xi, J., Zhao, T., Wang, D. & Shuai, Z. “Tunable Electronic Properties of TwoDimensional Transition Metal Dichalcogenide Alloys: A First-Principles Prediction”. J. Phys. Chem. Lett. (2013) 5, 285–291.

[42] Chen, Y. et al. “Tunable Band Gap Photoluminescence from Atomically Thin Transition-Metal Dichalcogenide Alloys”. ACS Nano (2013) 7, 4610–4616.

[43] Li-Yong Gan, Qingyun Zhang, Yu-Jun Zhao, Yingchun Cheng, Udo Schwingenschlögl Sci Rep. 2014; 4: 6691

[44] Kobayashi, Yu, et al. "Bandgap-tunable lateral and vertical heterostructures based on monolayer Mo1-xWxS2 alloys." Nano Research 8.10 (2015): 3261-3271.

[45] V. Popescu and A. Zunger “Extracting E versus k effective band structure from supercell calculations on alloys and impurities” Phys. Rev. B (2012) 85, 085201

APPENDICES

APPENDIX A

QUANTUM ESPRESSO

This section will talk about software, which is an integrated suite of Open-Source computer codes for electronic structure calculations and materials modeling at the nanoscale. It is based on the Density Functional Theory with plane-waves basis set and pseudopotentials, call as “Quantum ESPRESSO”. The Quantum ESPRESSO has evolved into a distribution of independent and inter-operable codes in the spirit of an open source project. The Quantum ESPRESSO distribution consists of a “historical” core set of components, and a set of plug-ins that perform more advanced tasks, plus a number of third-party packages designed to be inter operable with the core components. Researchers active in the field of electronic structure calculations are encouraged to participate in the project by contributing their own codes or by implementing their own ideas into existing codes [20].

A lot of things about electronical and physical properties was been calculated by the Quantum ESPRESSO. But in this work, we will focus on ground state calculations, structural optimization and band structure calculation. This section shows about input file description and required input data for any calculations on this thesis. By program: pw.x on Quantum ESPRESSO. The required structure of input data on pw.x are

(1) &CONTROL, which is general variables controlling the run to point out what the program pw.x should do. The most important part is task, that determine what the program will calculate. For this thesis, the tasks to be performed are (1.1) ‘scf’ performs a single-point (fixed-ion) calculation, this task should be the first thing to do for any first-principle studies. (1.2) ‘nscf’ performs a non-SCF calculation with the desired k-point grid that lead to further processing, bands and density of state calculation. (1.3) ‘bands’ performs a bands structure calculation that base on the desired k-point. (1.4) ‘vc-relax’ performs a variable-cell relaxation for studied system.

(2) &SYSTEM, structural information on the system under investigation. It is specified depend on the studied system (likes Bravais-lattice index, Kinetic energy cutoff for wave functions, Kinetic energy cutoff for charge density and potential etc.)

(3) &ELECTRONS, which is input variables that control the algorithms used to reach the self-consistent solution of Kohn-Sham equations for the electrons in the system.

And there are three mandatories for specify the system.

(4) ATOMIC_SPECIES describe name, mass and pseudopotential used for each atomic species present in the system.

(5) ATOMIC_POSITIONS describe type and coordinates of each atom in the unit cell of the system.

(6) K-POINTS describe coordinates and weights of the k-points used for the Brillouin zone integration. If it is set to 'automatic' then automatically generated uniform grid of k-points as in Monkhorst Pack grids.

There are a lot of description of pw.x for more information please visit,

http://www.quantum-espresso.org/wp-content/uploads/Doc/INPUT_PW.html#idm140629871987664

The next page shows structure of the input data with minimal require for program pw.x calculation on the Quantum ESPRESSO package.

Structure of the input data

&CONTROL

...

/

&SYSTEM

...

/

&ELECTRONS

...

/

ATOMIC_SPECIES

X Mass_X PseudoPot_X

Y Mass_Y PseudoPot_Y

ATOMIC_POSITIONS { alat | bohr | crystal | angstrom | crystal_sg }

X 0.0 0.0 0.0 {if_pos(1) if_pos(2) if_pos(3)}

Y 0.5 0.0 0.0

K_POINTS { tpiba | automatic | crystal | gamma | tpiba_b | crystal_b | tpiba_c | crystal_c }

if (automatic)

nk1, nk2, nk3, k1, k2, k3

if (not automatic)

nk_s

xk_x, xk_y, xk_z wk (weight of k-points)

APPENDIX B

BAND STRUCTURE UNFOLDING

In chapter 5, we need to construct electronic band structure from $Mo_{1-x}W_xS_2$ (3x3x1 supercell). For plane-wave based calculations the band structure obtained by the supercell calculation was represented by the Brillouin zone of a primitive cell so that the periodicity of calculated band structure may be completely different from the primitive cell. The band structure of the supercell calculation is in general quite cluttered. However, the band structure of supercell calculations is usually performed in order to allow for slight reformation of the crystal structure (likes alloy in this thesis). The electronic band structure of the primitive cell is preserved. To this extent, unfolding the band structure of the supercell to the one of the primitive cell by consider the case where the basis vector of the supercell and primitive cell satisfy

$$\boldsymbol{A} = M \cdot \boldsymbol{a} \tag{A.1}$$

where $\boldsymbol{A}$ and $\boldsymbol{a}$ are matrices with the cell basis vectors and $\boldsymbol{M}$ is the transformation matrix. Likewise, so in reciprocal space should be

$$\boldsymbol{B} = M^{-1} \cdot \boldsymbol{b} \tag{A.2}$$

Then given a $\boldsymbol{k}$ in the primitive Brillouin zone there is only a $\boldsymbol{K}$ in the supercell Brillouin zone to which it folds into. The two vectors are related by a reciprocal lattice vector $\boldsymbol{G}$ in the supercell Brillouin zone describe by

$$\boldsymbol{k} = \boldsymbol{K} + \boldsymbol{G} \tag{A.3}$$

The spectral function of the primitive cell calculation evaluates from eigenvalues and eigenfunctions of the supercell calculation one. Such a spectral function can be calculated as follow

$$A(\boldsymbol{k}, \epsilon) = \sum_m P_{\boldsymbol{K}_m}(\boldsymbol{k}) \delta\left(\epsilon_{\boldsymbol{K}_m} - \epsilon\right) \tag{A.4}$$

and from delta function, $P_{\boldsymbol{K}_m}(\boldsymbol{k})$ are the weights defined by

$$P_{\boldsymbol{K}_m}(\boldsymbol{k}) = \sum_n |\langle \boldsymbol{K}_m | \boldsymbol{k}_n \rangle|^2 \tag{A.5}$$

Obviously shows that given information about how much $|\boldsymbol{k}_n\rangle$ is preserved $|\boldsymbol{K}_n\rangle$. From the expression above, it seems that calculating the weights requires the information of primitive cell eigenstates. However, V.Popescu and A.Zunger [45] show that weights can be found using only supercell quantities, now using Fourier transformation we get

$$P_{\boldsymbol{K}_m}(\boldsymbol{k}) = \sum_{\boldsymbol{G}} \left| C_{\boldsymbol{K}_m}(\boldsymbol{G} + \boldsymbol{k} - \boldsymbol{K}) \right|^2 \qquad (A.6)$$

where $\boldsymbol{C}_{\boldsymbol{K}_m}$ are the Fourier coefficients of the eigenstate $\boldsymbol{K}_m$ and $\boldsymbol{G}$ is reciprocal space vectors of the supercell, specifically the ones that match the reciprocal space vectors of the primitive cell.

Band structure calculation in this thesis was unfolded. The unfolding has been performed using the BandUP code. The BandUP is a code that allows you to obtain a primitive cell representation of the band structure of systems simulated using supercells. The unfolding of the bands is performed as described in the following works [39, 40]. No explicit calculations involving the reference primitive cell are needed. One only needs to know the primitive cell vectors to determine the geometric unfolding relations. BandUP checks the symmetries of both supercell and reference primitive cell to (1) reduce the number of necessary k-points to a minimum thus reducing the space required to store wavefunction files, and (2) produce properly symmetry-averaged effective unfolded band structures (EBS) when the symmetry of the supercell is different from the one of the primitive cell. This is handy when defects, impurities and/or other types of perturbations are present.

APPENDIX C

SQS WITH PYTHON

According to the Chapter 3, the basic idea for programing of Special Quasirandom Structure method. In this section, we will introduce a programing language that was used for design SQS method. By using python, a programing language with dynamic semantics, provides a high-level built in data structures. That easy to learn syntax emphasizes and therefore reduces the time of program construction. Comparing python to other language such as Java or C++. In practice, the choice of a programming language is often dictated by time to develop code, speed of program running and convenience for apply coding program to solve problem. For Java, python programs are generally expected to run slower than Java programs, but they also take much less time to develop. Python programs are typically 3 times shorter than equivalent Java programs. This difference can be attributed to Python's built-in high-level data types and its dynamic typing. As same as C++, even C++ run faster than python but python is often 10 times shorter than equivalent C++ code because of C++ has not a high-level built in data structures. Python shines as a glue language, used to combine components written in C++. Python is used in many application domains, now we will integrate python language and idea of SQS method.

The first step of modeling materials. We store input information (a cell parameter and atomic positions) by using dictionary data type. Python “dictionary” is a data structure. It is best to think of a dictionary as an unordered set of {key: value} pairs, with the requirement that the keys are unique (within one dictionary). A pair of braces creates an empty dictionary: {}. Placing a comma-separated list of {key: value} pairs within the braces adds initial {key: value} pairs to the dictionary; this is also the way dictionaries are written on output. The main operations on a dictionary are storing a value with some key and extracting the value given the key. For example, in Figure C. 1 if we call A or B keys then we will know every number of atom that are same type

as A (e.g. call A keys then the program return value [1, 2, 3, 7, 8, 9, 13, 14, 15] that are list of atoms). Then we can collect or calculate data that we need (distance of each atoms, assign pseudo-spin, construct figures, etc.).

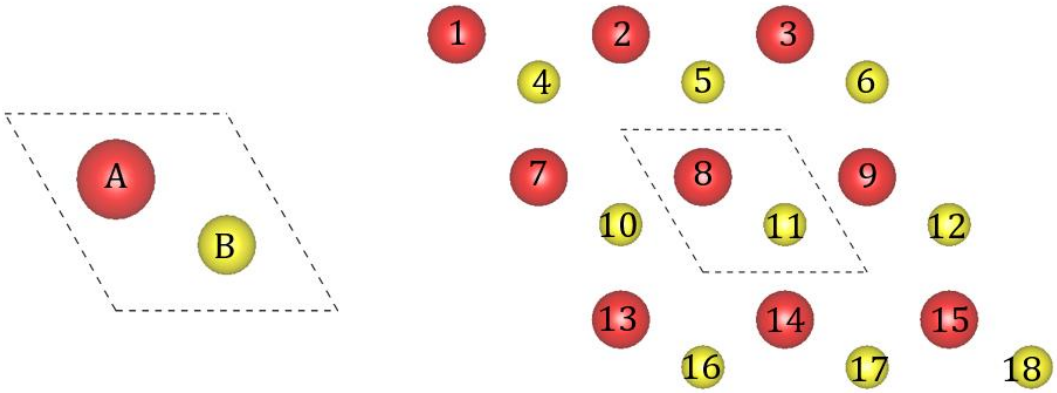

Figure C. 1 A representation of data structure in python, (left) input information as keys, (right) values of dictionaries that represent number of atom in the system studies.

The next step, we want the SQS program compute the product of the pseudo-spin by figures call as correlation function $\prod_{k,m} \boldsymbol{S}$. The correlation function for each figure is calculate by assign value on atom in the previous step. Then matching up with the same figures for each atom in the primitive cell. Those data have been used by calculation average of the correlation functions.

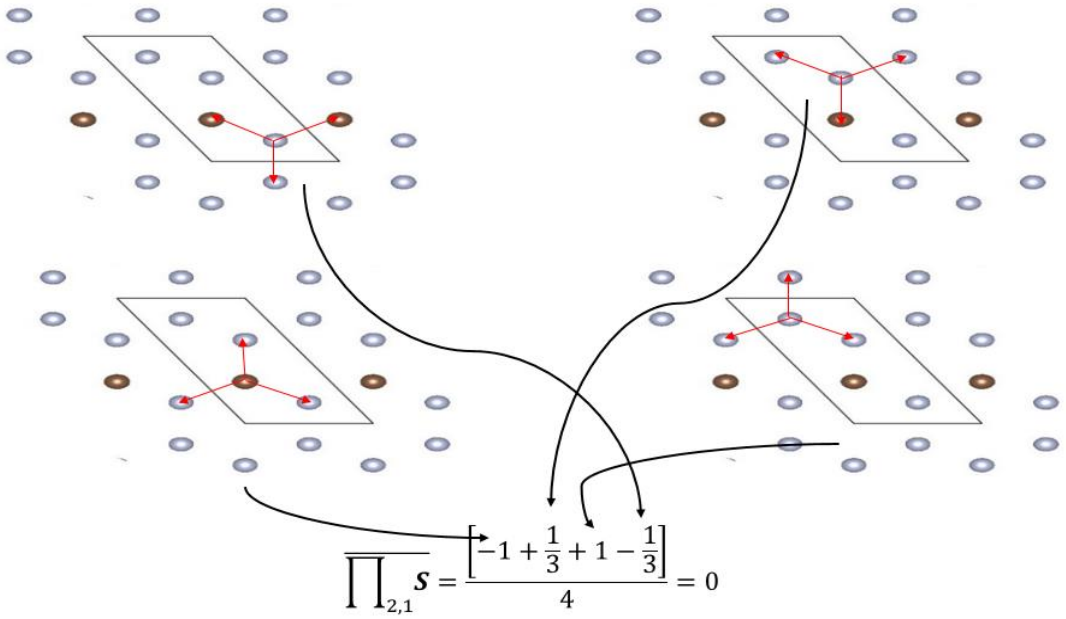

Figure C. 2 An example diagram of calculate average correlation function of figure (2,1).

VITA

Mr. Wirunti Pungtrakoon was born on 18 November 1992. He graduated from Nakprasith school. Then he got Bachelor of Science in physics (B.Sc. Physics) from Chulalongkorn University in 2014. His senior project in B.Sc. is on the hydrogen storage on the 2D materials using first-principle calculation. Afterwards, he continued Master of Science in physics (M.Sc. physics) and worked in the Extreme Condition Physics Research Laboratory (ECPRL) at Chulalongkorn University. The advisor in M.Sc. is assoc. prof. Thiti Bovornratanaraks and the co-advisor assoc. prof. Udomsilp Pinsook in the subject of model of alloy molybdenum tungsten disulfide structure using Special Quasirandom Structure method.